UNIVERSITY OF CALIFORNIA, SAN DIEGO

Wave Propagation in Uniformly Pre-twisted Isotropic Beams with Uniform Cross-sections

A Thesis submitted in partial satisfaction of the

requirements for the degree Master of Science

in

Engineering Sciences (Mechanical Engineering)

by

Yupeng Zhang

Committe in charge:

Professor Hidenori Murakami , Chair
Professor Nathan Delson
Professor Vlado Lubarda

2012

The Thesis of Yupeng Zhang is approved and it is acceptable in quality and form for publication on microfilm and electronically:

Chair

University of California, San Diego 2012

Dedication

To Ms. Pricilla Chan, Homestead High's most dedicated career counselor who devoted her life to providing care and guidance for young souls in need. Your legacy lives on in every acceptance letter, every diploma, every graduation song and every proud smile on our faces.

Epigraph

There are two primary choices in life, to accept conditions as they exist, or accept the responsibility for changing them.

-Denis waitley

Table of Contents

List of Figures

List of Tables

Acknowledgments

I would like to thank my advisor, Dr. Murakami, for his guidance, teaching and extraordinary patience despite my trying ways. Without whom, this thesis would not have been possible.

I would also like to thank my friends and family for standing by me and believing in me during this difficult time. The support I have received, both emotional and tangible, made a world of difference, for that, I am truly grateful.

Last but not least, I would like to thank Dr. Lubarda and Dr. Delson for serving on my defense committee, offering their valuable time and suggestions.

ABSTRACT OF THE THESIS

Wave Propagation in Uniformly Pre-twisted Isotropic Beams with Uniform Cross-sections

by

Yupeng Zhang

Master of Science in Engineering Sciences (Mechanical Engineering)

University of California, San Diego, 2012

Professor Hidenori Murakami, Chair

In this thesis, harmonic wave propagation in pre-twisted beams with arbitrary rate of uniform pre-twist was investigated utilizing the three-dimensional theory of elasto-dynamics expressed in the curvilinear coordinates. Harmonic wave propagation in the axial direction defines an eigen-value problem over the cross-section of the beam. By developing a finite element code to solve generalized eigenvalue problem, the eigenvalues and corresponding eigenmodes were computed to elucidate the effect of pre-twist on phase velocities and mode shapes. Lowest four modes which describe

longitudinal, torsional, minor-axis bending and major-axis bending deformations were numerically investigated for two rectangular cross-sections with aspect ratios: 4:1 and 2:1 and an elliptic cross-section with aspect ratio of 5:1. The resulting phase velocity spectra are observed to be affected by the pre-twist and are valuable in the assessment of the accuracy of beam models used for dynamic analysis of pre-twisted beams. In addition, the resulting mode shapes consistently demonstrate the effect of pre-twist on the coupling of torsion-extension and the minor-major bending stiffnesses.

1 Introduction

Beams of twisted form with respect to their longitudinal axes in the unstressed state, referred to as pre-twisted beams, describe structures such as rotor blades or turbine blades. In such pre-twisted beams, it has been experimentally observed that extensional force causes untwist, and similarly a torsional moment causes elongation or contraction depending on whether original twist is decreased or increased.

An initial successful attempt of modeling the deformation of pre-twisted beams by using beam theories resorted to an ingenious intuition, known as Wagners hypothesis (Buckley [10], 1914; Wagner [13], 1936). The hypothesis is that the beam consists of straight fibers in the untwisted state. These fibers run through the cross-section in a helically twisted fashion when the beam is given an initial twist in the unstressed state. If one assumes that axial stress is only carried by the fibers, axial tension acted on helical fibers induces untwisting of the helical fibers.

Mathematical derivation of pre-twisted beam equations incorporating the displacement assumptions on the cross-section has to be performed using curvilinear coordinates, which describe the pre-twist of the beam (Washizu [14], 1964). In order to include the untwisting effect under tension, warping of cross-sections has to be included a priori using the curvilinear coordinates (Hodge [11], 1980).

For pre-twisted beams of elliptic cross-sections, semi-inverse analyses were performed for torsional deformation and bending deformation utilizing the three-dimensional theory of elasticity using the curvilinear coordinates. Okubo [9] (1951)

investigated the torsion and stretching of pre-twisted beams of elliptic cross-section for a small rate of initial twist employing the asymptotic expansion with respect to the small rate of initial twist along the axis of the beam. He computed the torsion-extension and tension-untwisting coupling terms based upon the three-dimensional theory of elasticity ending the controversy about the amplitude of the coupling effect.

With respect to the bending deformation, the effect of pre-twist on the bending stiffness was investigated by Maunder and Reissner [12] (1957) and Goodier and Griffin [5] (1969). Using the shallow shell theory of a pre-twisted beam of rectangular cross-section, which was approximated as a thing shallow shell, Maunder and Riessner (1957) reported that the bending stiffness with the major axis reduced compared to the untwisted beam, while the bending stiffness with the minor axis increased compared to the untwisted beam. For a pre-twisted beam of elliptic cross-section, Goodier and Griffin (1969) utilized the equilibrium equations for the curvilinear coordinates and performed a semi-inverse analysis to obtain the same effect on the minor and major bending stiffnesses analytically for a small rate of pre-twist. The semi-inverse analyses of Okubo and Goodier and Griffin (1969) were performed only for a small rate of pre-twist by keeping the linear term in the asymptotic expansion with respect to the small rate of pre-twist. These three-dimensional analyses utilizing the theory of elasticity employing the semi-inverse method or the shallow shell theory presented the stiffness or compliance for the beam models to incorporate the effect of pre-twist. However, beam models developed for static analyses may not extend smoothly to dynamic analyses.

Dynamics analyses of pre-twisted beams have been investigated by using Euler-Bernoulli or Timshenko beam models to computed natural frequency of cantilever beams (Banerjee [6], 2004). Yet, the fidelity of beam models has not been assessed by using three-dimensional theory of elasticity.

In this thesis, harmonic wave propagation of pre-twisted beams with arbitrary rate of uniform pre-twist was investigated utilizing the three-dimensional theory of elasto-dynamics expressed in the curvilinear coordinates to represent helically pre-twisted beams. Harmonic wave propagation in the axial direction defines an eigenvalue problem over the cross-section of the beam involving hermitian matrices. By developing a finite element code to solve generalized eigenvalue problem involving hermitian stiffness matrix and real symmetric mass matrix, the eigenvalues and corresponding eigenmodes were computed to elucidate the effect of pre-twist on phase velocities and mode shapes. Lowest four modes which describe longitudinal, torsional, minor-axis bending, and major-axis bending deformations were numerically investigated for two rectangular cross-sections with aspect ratios: 4:1 and 2:1 and an elliptic cross-section with aspect ratio of 5:1.

The mode shapes show consistently the effect of pre-twist on the coupling of torsion-extension and the coupling of minor-major bending stiffnesses as Okubo (1951) and Goodier and Griffin (1969) reported.

The resulting phase velocity spectra are useful to assess the accuracy of beam models used for dynamic analysis of pre-twisted beams. Furthermore, the mode shapes are useful to check the validity of the semi-inverse boundary value problems defined over the cross-section to develop pre-twisted beams models used for dynamic analyses.

2 Derivation of Three Dimensional Strain - Displacement Relations

In order to investigate harmonic wave propagation in a pretwisted beam with uniform cross-section, it is necessary to derive equations of motion with respect to a curvilinear coordinate system which describes the pre-twisted cross-sections by helices. To this end, we first derive strain-displacement relation and utilize the principle of virtual work to obtain the equations of motion for the curvilinear coordinate system. The resulting equations must be expressed in terms of physical components, instead of tensor components.

2.1 Defining a Curvilinear Coordinate System for Pre-Twisted Beam

Let x^1, x^2, x^3 be the base rectangular cartesian coordinates where x^3 axis coincides with the center line of the pre-twisted beam. The cross-section at $x^3 = \text{constant}$ is rotated relative to the cross-section at the origin by an angle αx^3, where α is the uniform rate of pre-twist. The x^1 and x^2 axes coincide with the principle axes of the cross-section at $x^3 = 0$, as illustrated in Figure(1).

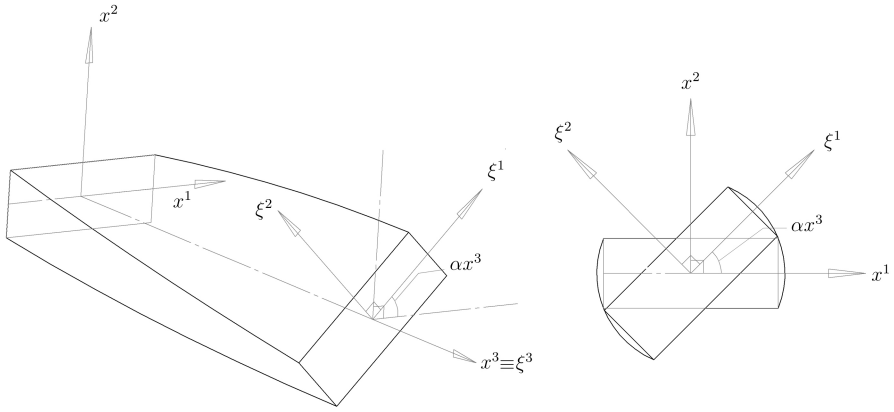

Figure 1: Curvilinear Coordinate System

The curvilinear coordinates system ξ^1, ξ^2, ξ^3 is selected in such a way that $\xi^3 = x^3$ and the ξ^1 and ξ^2 coincide locally with the principal axes of the cross-section.

The corresponding coordinate transfomration is expressed as:

$$\begin{bmatrix} \xi^1 \\ \xi^2 \\ \xi^3 \end{bmatrix} = \begin{bmatrix} \cos \alpha x^3 & \sin \alpha x^3 & 0 \\ -\sin \alpha x^3 & \cos \alpha x^3 & 0 \\ 0 & 0 & 1 \end{bmatrix} \begin{bmatrix} x^1 \\ x^2 \\ x^3 \end{bmatrix} \tag{1}$$

2.2 Method of Differential Geometry / Tensor Analysis

For the curvilinear coordinate system defined in (1), the covariant base vectors $\boldsymbol{g}_i = \frac{\partial \boldsymbol{x}}{\partial \xi^i}$. The covariant metric tensor, g_{ij} is defined as:

$$ds^2 = g_{ij}(\xi^1, \xi^2, \xi^3) d\xi^i d\xi^j \tag{2}$$

$$g_{ij}\left(\xi^1, \xi^2, \xi^3\right) =< \boldsymbol{g}_i \cdot \boldsymbol{g}_j >= \frac{\partial x^m}{\partial \xi^i} \frac{\partial x^m}{\partial \xi^j} \tag{3}$$

where summation convention for repeated indices is implied.

$$[g_{ij}] = \begin{bmatrix} 1 & 0 & -\alpha\xi^2 \\ 0 & 1 & \alpha\xi^1 \\ -\alpha\xi^2 & \alpha\xi^1 & 1+\alpha^2((\xi^1)^2+(\xi^2)^2) \end{bmatrix} \tag{4}$$

The determinant of the matrix of g_{ij} is $g = det[g_{ij}] = 1$

The corresponding contravariant metric tensor g^{ij} is defined as follows:

$$[g^{ij}] = [g_{ij}]^{-1}$$

$$[g^{ij}] = \begin{bmatrix} 1+(\alpha\xi^2)^2 & -\alpha^2\xi^1\xi^2 & \alpha\xi^2 \\ -\alpha^2\xi^1\xi^2 & 1+(\alpha\xi^1)^2 & -\alpha\xi^1 \\ \alpha\xi^2 & -\alpha\xi^1 & 1 \end{bmatrix} \tag{5}$$

The contravariant base vector $\boldsymbol{g}^i$ is defined as:

$$\boldsymbol{g}^i = g^{ik}\boldsymbol{g}_k \tag{6}$$

and the following orthogonality relationship holds (Green and Zerna [15],1954):

$$\boldsymbol{g}_r \times \boldsymbol{g}_s = \sqrt{g}\varepsilon_{rst}\boldsymbol{g}^t \tag{7}$$

where ε_{rst} is the permutation symbol.

Referring to (3) and (4):

$$g_{11} =< \boldsymbol{g}_1 \cdot \boldsymbol{g}_1 >= 1$$

$$g_{22} =< \boldsymbol{g}_2 \cdot \boldsymbol{g}_2 >= 1$$

$$g_{12} =< \boldsymbol{g}_1 \cdot \boldsymbol{g}_2 >= 0$$

it is observed that $\boldsymbol{g}_1$ and $\boldsymbol{g}_2$ are unit vectors and orthogonal to each other

Utilizing this orthonormal relationship, a moving frame $\hat{\mathbf{e}} \equiv (\hat{\mathbf{e}}_\mathbf{1}, \hat{\mathbf{e}}_\mathbf{2}, \hat{\mathbf{e}}_\mathbf{3})$ can be established as:

$$\begin{aligned} \hat{\mathbf{e}}_1 &= \boldsymbol{g}_1 \\ \hat{\mathbf{e}}_2 &= \boldsymbol{g}_2 \end{aligned} \tag{8}$$

and using equation (6):

$$\hat{\mathbf{e}}_3 = \hat{\mathbf{e}}_1 \times \hat{\mathbf{e}}_2 = \boldsymbol{g}_1 \times \boldsymbol{g}_2 = \boldsymbol{g}^\mathbf{3} = g^{3k} g_k \tag{9}$$

From (8) and (9), the local orthonormal frame $\hat{\mathbf{e}}$ is related to the covariant base vector as:

$$\begin{bmatrix} \hat{\mathbf{e}}_1 & \hat{\mathbf{e}}_2 & \hat{\mathbf{e}}_3 \end{bmatrix} = \begin{bmatrix} \boldsymbol{g}_1 & \boldsymbol{g}_2 & \boldsymbol{g}_3 \end{bmatrix} \begin{bmatrix} 1 & 0 & \alpha\xi^2 \\ 0 & 1 & -\alpha\xi^1 \\ 0 & 0 & 1 \end{bmatrix} \tag{10}$$

The inverse to (6) is expressed as:

$$\boldsymbol{g}_i = g_{ij} \boldsymbol{g}^j$$

and in expanded form:

$$\begin{bmatrix} \boldsymbol{g}_1 & \boldsymbol{g}_2 & \boldsymbol{g}_3 \end{bmatrix} = \begin{bmatrix} \boldsymbol{g}^1 & \boldsymbol{g}^2 & \boldsymbol{g}^3 \end{bmatrix} \begin{bmatrix} 1 & 0 & -\alpha\xi^2 \\ 0 & 1 & \alpha\xi^1 \\ -\alpha\xi^2 & \alpha\xi^1 & 1+\alpha^2((\xi^1)^2+(\xi^2)^2) \end{bmatrix} \tag{11}$$

The displacement vector is expressed with respect to both covariant and controvariant base vectors:

$$\mathbf{u} = u_i \boldsymbol{g}^i = u^k \boldsymbol{g}_k \tag{12}$$

where u_i and u^k are covariant and contravariant components of the displacement vector. The displacement components are not physical components unless the local coordinates are orthonormal.

Let physical displacement components associated with orthonormal frame $\hat{\mathbf{e}}$ be $\hat{u_1}, \hat{u_2}, \hat{u_3}$

$$\mathbf{u} = \begin{bmatrix} \boldsymbol{g}_1 & \boldsymbol{g}_2 & \boldsymbol{g}_3 \end{bmatrix} \begin{bmatrix} u^1 \\ u^2 \\ u^3 \end{bmatrix} = \begin{bmatrix} \hat{\mathbf{e}}_1 & \hat{\mathbf{e}}_2 & \hat{\mathbf{e}}_3 \end{bmatrix} \begin{bmatrix} \hat{u_1} \\ \hat{u_2} \\ \hat{u_3} \end{bmatrix} = \begin{bmatrix} \boldsymbol{g}^1 & \boldsymbol{g}^2 & \boldsymbol{g}^3 \end{bmatrix} \begin{bmatrix} u_1 \\ u_2 \\ u_3 \end{bmatrix} \tag{13}$$

From equation (10) the relation between displacement components in the covariant basis and the local orthonormal frame $\hat{\mathbf{e}}$ is established as:

$$\begin{bmatrix} u^1 \\ u^2 \\ u^3 \end{bmatrix} = \begin{bmatrix} 1 & 0 & \alpha\xi^2 \\ 0 & 1 & -\alpha\xi^1 \\ 0 & 0 & 1 \end{bmatrix} \begin{bmatrix} \hat{u_1} \\ \hat{u_2} \\ \hat{u_3} \end{bmatrix} \tag{14}$$

From equation (11) the covariant and controvariant displacement components are related by controvariant metric tensor as:

$$\begin{bmatrix} u_1 \\ u_2 \\ u_3 \end{bmatrix} = \begin{bmatrix} 1 & 0 & -\alpha\xi^2 \\ 0 & 1 & \alpha\xi^1 \\ -\alpha\xi^2 & \alpha\xi^1 & 1+\alpha^2((\xi^1)^2+(\xi^2)^2) \end{bmatrix} \begin{bmatrix} u^1 \\ u^2 \\ u^3 \end{bmatrix} \tag{15}$$

Combining equation (14) and (15), the relation between covariant displacement component and physical displacement components becomes:

$$\begin{bmatrix} u_1 \\ u_2 \\ u_3 \end{bmatrix} = \begin{bmatrix} 1 & 0 & -\alpha\xi^2 \\ 0 & 1 & \alpha\xi^1 \\ -\alpha\xi^2 & \alpha\xi^1 & 1+\alpha^2((\xi^1)^2+(\xi^2)^2) \end{bmatrix} \begin{bmatrix} 1 & 0 & \alpha\xi^2 \\ 0 & 1 & -\alpha\xi^1 \\ 0 & 0 & 1 \end{bmatrix} \begin{bmatrix} \hat{u_1} \\ \hat{u_2} \\ \hat{u_3} \end{bmatrix}$$

$$\begin{bmatrix} u_1 \\ u_2 \\ u_3 \end{bmatrix} = \begin{bmatrix} 1 & 0 & 0 \\ 0 & 1 & 0 \\ -\alpha\xi^2 & \alpha\xi^1 & 1 \end{bmatrix} \begin{bmatrix} \hat{u_1} \\ \hat{u_2} \\ \hat{u_3} \end{bmatrix} \tag{16}$$

The small-strain tensor is given as:

$$\boldsymbol{\varepsilon} = \boldsymbol{g}^i \otimes \varepsilon_{ij}\boldsymbol{g}^j \tag{17}$$

and

$$\varepsilon_{ij} = \frac{1}{2}(u_i|_j + u_j|_i) = \frac{1}{2}(u_{i,j} + u_{j,i} - 2\Gamma^m_{ij}u_m) \tag{18}$$

Where $|_i$ denotes covariant differentiation with respect to ξ^i and $()_{,i}$ denotes partial differentiation with respect to ξ^i. Γ^m_{ij} is the christoffel symbol.

Christoff symbol are obtained from equation:

$$\Gamma_{ij}^{m} = \frac{1}{2} g^{mk} \left(\frac{\partial g_{kj}}{\partial \xi^{i}} + \frac{\partial g_{ik}}{\partial \xi^{j}} + \frac{\partial g_{ij}}{\partial \xi^{k}} \right) \tag{19}$$

The non-zero Christoffel symbols are:

$$\begin{aligned} &\Gamma_{13}^{2} = \alpha \qquad \Gamma_{23}^{1} = -\alpha \qquad \Gamma_{32}^{1} = -\alpha \\ &\Gamma_{33}^{1} = \alpha^{2} \xi^{1} \qquad \Gamma_{31}^{2} = \alpha \qquad \Gamma_{33}^{2} = -\alpha^{2} \xi^{2} \end{aligned} \tag{20}$$

Substituting (20) into (18), the covariant strain components become:

$$\begin{aligned} \varepsilon_{11} &= u_{1,1} \\ \varepsilon_{22} &= u_{2,2} \\ \varepsilon_{33} &= u_{3,3} + \alpha^{2} \xi^{1} u_{1} + \alpha^{2} \xi^{2} u_{2} \\ 2\varepsilon_{23} &= 2\varepsilon_{32} = u_{3,2} + u_{2,3} + 2\alpha u_{1} \\ 2\varepsilon_{13} &= 2\varepsilon_{31} = u_{1,3} + u_{3,1} - 2\alpha u_{2} \\ 2\varepsilon_{12} &= 2\varepsilon_{21} = u_{1,2} + u_{2,1} \end{aligned} \tag{21}$$

In terms of physical components by relation (16):

$$\begin{aligned} \varepsilon_{11} &= \hat{u}_{1,1} \\ \varepsilon_{22} &= \hat{u}_{2,2} \\ \varepsilon_{33} &= -\alpha \xi^{2} \hat{u}_{1,3} + \alpha \xi^{1} \hat{u}_{2,3} + \hat{u}_{3,3} + \alpha^{2} \xi^{1} \hat{u}_{1} + \alpha^{2} \xi^{2} \hat{u}_{2} \\ 2\varepsilon_{23} &= 2\varepsilon_{32} = \hat{u}_{3,2} + \hat{u}_{2,3} + \alpha \hat{u}_{1} - \alpha \xi^{2} \hat{u}_{1,2} + \alpha \xi^{1} \hat{u}_{2,2} \\ 2\varepsilon_{13} &= 2\varepsilon_{31} = \hat{u}_{1,3} + \hat{u}_{3,1} - \alpha \hat{u}_{2} - \alpha \xi^{2} \hat{u}_{1,1} + \alpha \xi^{1} \hat{u}_{2,1} \\ 2\varepsilon_{12} &= 2\varepsilon_{21} = \hat{u}_{1,2} + \hat{u}_{2,1} \end{aligned} \tag{22}$$

From (10) and (11):

$$\begin{bmatrix} \hat{\mathbf{e}}_1 & \hat{\mathbf{e}}_2 & \hat{\mathbf{e}}_3 \end{bmatrix} = \begin{bmatrix} \boldsymbol{g}^1 & \boldsymbol{g}^2 & \boldsymbol{g}^3 \end{bmatrix} \begin{bmatrix} 1 & 0 & 0 \\ 0 & 1 & 0 \\ -\alpha\xi^2 & \alpha\xi^1 & 1 \end{bmatrix} \tag{23}$$

inverse of the above relation is:

$$\begin{bmatrix} \boldsymbol{g}^1 & \boldsymbol{g}^2 & \boldsymbol{g}^3 \end{bmatrix} = \begin{bmatrix} \hat{\mathbf{e}}_1 & \hat{\mathbf{e}}_2 & \hat{\mathbf{e}}_3 \end{bmatrix} \begin{bmatrix} 1 & 0 & 0 \\ 0 & 1 & 0 \\ \alpha\xi^2 & -\alpha\xi^1 & 1 \end{bmatrix} \tag{24}$$

$$\boldsymbol{g}^i = \hat{\mathbf{e}}_m \hat{Q}^{mi} \tag{25}$$

Substitute (25) into (17)

$$\boldsymbol{\varepsilon} = \hat{\mathbf{e}}_m \hat{Q}^{mi} \otimes \varepsilon_{ij} \hat{Q}^{nj} \hat{\mathbf{e}}_n \tag{26}$$

Physical strain components from the above are:

$$\hat{\varepsilon}_{mn} = \hat{Q}^{mi} \varepsilon_{ij} \hat{Q}^{nj} \tag{27}$$

And in expanded form, physical strain components are expressed in terms of physical displacement components:

$$\hat{\varepsilon}_{11} = \hat{u}_{1,1}$$

$$\hat{\varepsilon}_{22} = \hat{u}_{2,2}$$

$$\hat{\varepsilon}_{33} = \hat{u}_{3,3} + \alpha\xi^2\hat{u}_{3,1} - \alpha\xi^1\hat{u}_{3,2}$$

$$2\hat{\varepsilon}_{23} = \hat{u}_{3,2} + \hat{u}_{2,3} + \alpha\xi^2\hat{u}_{2,1} - \alpha\xi^1\hat{u}_{2,2} + \alpha\hat{u}_1$$

$$2\hat{\varepsilon}_{13} = \hat{u}_{1,3} + \hat{u}_{3,1} + \alpha\xi^2\hat{u}_{1,1} - \alpha\xi^1\hat{u}_{1,2} - \alpha\hat{u}_2$$

$$2\hat{\varepsilon}_{12} = \hat{u}_{2,1} + \hat{u}_{1,2} \tag{28}$$

2.3 Method of Coordinate Transformation

The following derivation follows closely to the work of Goodier and Griffin [5]. Observing that the strain components on an elementary parallelipiped with edges parallel to the local ξ^1, ξ^2, x^3 coordinates (Note that local base vectors are now equivalent to the $\hat{\mathbf{e}}^i$ coordinate as constructed in previous section) written as the local strain component $\hat{\varepsilon}_{ij}$ are related to the strain components $\tilde{\varepsilon}_{ij}$ of the x^1, x^2, x^3 coordinates by the well known formulas of transformation from one orthogonal cartesian system to another. With the scheme described in (1).

The transformation matrix Q is define as follows:

$$[Q] = \begin{bmatrix} \cos\alpha x^3 & -\sin\alpha x^3 & 0 \\ \sin\alpha x^3 & \cos\alpha x^3 & 0 \\ 0 & 0 & 1 \end{bmatrix} \tag{29}$$

And displacement transformation relation is:

$$\left\{\hat{u}\right\} = [Q]^T \left\{\tilde{u}\right\} \tag{30}$$

Where $\hat{u}_i$ are displacements with respect to the local ξ^1, ξ^2, x^3 coordinates and $\tilde{u}_i$ are displacements with respect to $\boldsymbol{x}^i$. Transformation of Strain tensor is expressed as:

$$[\hat{\varepsilon}] = [Q]^T[\tilde{\varepsilon}][Q] \tag{31}$$

Strain displacement relation in the x^1, x^2, x^3 coordinate is defined as:

$$\tilde{\varepsilon}_{ij} = \frac{1}{2}(\frac{\partial \tilde{u}_i}{\partial x^j} + \frac{\partial \tilde{u}_j}{\partial x^i}) \tag{32}$$

Which can also be written as:

$$\tilde{\varepsilon}_{ij} = \frac{1}{2}(\frac{\partial \tilde{u}_i}{\partial \xi^k}\frac{\partial \xi^k}{\partial x^j} + \frac{\partial \tilde{u}_j}{\partial \xi^k}\frac{\partial \xi^k}{\partial x^i}) \tag{33}$$

Using equation (1) and (30), substitute all displacements of (33) with corresponding local terms using (30). The strain tensor with respect to $\boldsymbol{x}^i$ coordinates can then be written with local components. Next a coordinate transformation described in (31) is performed to obtain the same strain-displacement relations (28).

3 Derivation of Three Dimensional Equations Of Motion

Having the strain displacement relation, the three dimensional equations of motion can be obtained via the principal of virtual work:

$$\int_v (\delta\hat{\varepsilon}_{ij}\hat{\sigma}_{ij} - \delta\hat{u}_i\rho\ddot{\hat{u}}_i)dv = 0 \tag{34}$$

Where $\hat{\sigma}_{ij}$ is the stress components in local coordinate.

The variation of strain components, $\delta\hat{\varepsilon}_{ij}$, are:

$$\begin{aligned}
\delta\hat{\varepsilon}_{11} &= \delta\hat{u}_{1,1} \\
\delta\hat{\varepsilon}_{22} &= \delta\hat{u}_{2,2} \\
\delta\hat{\varepsilon}_{33} &= \delta\hat{u}_{3,3} + \alpha\xi^2\delta\hat{u}_{3,1} - \alpha\xi^1\delta\hat{u}_{3,2} \\
2\delta\hat{\varepsilon}_{23} &= \delta\hat{u}_{3,2} + \delta\hat{u}_{2,3} + \alpha\xi^2\delta\hat{u}_{2,1} - \alpha\xi^1\delta\hat{u}_{2,2} + \alpha\delta\hat{u}_1 \\
2\delta\hat{\varepsilon}_{13} &= \delta\hat{u}_{1,3} + \delta\hat{u}_{3,1} + \alpha\xi^2\delta\hat{u}_{1,1} - \alpha\xi^1\delta\hat{u}_{1,2} - \alpha\delta\hat{u}_2 \\
2\delta\hat{\varepsilon}_{12} &= \delta\hat{u}_{2,1} + \delta\hat{u}_{1,2}
\end{aligned} \tag{35}$$

The substitution of (35) into (34) and integration by parts with arbitrary variation of virtual displacements gives the equation of motion:

$$\hat{\sigma}_{11,1} + \hat{\sigma}_{12,2} + \hat{\sigma}_{13,3} + \alpha\xi^2\hat{\sigma}_{13,1} - \alpha\xi^1\hat{\sigma}_{13,2} - \alpha\hat{\sigma}_{32} = \rho\ddot{\hat{u}}_1 \tag{36}$$

$$\hat{\sigma}_{21,1} + \hat{\sigma}_{22,2} + \hat{\sigma}_{23,3} + \alpha\xi^2\hat{\sigma}_{23,1} - \alpha\xi^1\hat{\sigma}_{23,2} + \alpha\hat{\sigma}_{31} = \rho\ddot{\hat{u}}_2$$

$$\hat{\sigma}_{31,1} + \hat{\sigma}_{32,2} + \hat{\sigma}_{33,3} + \alpha\xi^2\hat{\sigma}_{33,1} - \alpha\xi^1\hat{\sigma}_{33,2} = \rho\ddot{\hat{u}}_3$$

These equations agree with those derived by Okubo [9] and Goodier [5].

4 Harmonic Wave Analysis

To study the dynamic response of pre-twisted beams, an analysis of harmonic waves traveling in the x^3 (=ξ^3) direction (without any boundary) is performed to obtain phase velocity spectra.

Let $[\hat{u}_i, \hat{\varepsilon}_{ij}, \hat{\sigma}_{ij}](\xi^1, \xi^2, x_3, t)$ be written in the form of

$$[\bar{u}_i, \bar{\varepsilon}_{ij}, \bar{\sigma}_{ij}](\xi^1, \xi^2; \omega, k) e^{(\sqrt{-1}kx^3 - \sqrt{-1}\omega t)} \tag{37}$$

where k is the wave number and ω is the angular frequency. The wave length Λ is obtained from wave number k as: $\Lambda = \frac{2\pi}{k}$

Substituting (37) into (36),the equations of motion for the harmonic wave propagation is obtained:

$$\begin{aligned}
&\bar{\sigma}_{11,1} + \bar{\sigma}_{12,2} + ik\bar{\sigma}_{13} + \alpha\xi^2\bar{\sigma}_{13,1} - \alpha\xi^1\bar{\sigma}_{13,2} - \alpha\bar{\sigma}_{32} = -\omega^2\rho\bar{u}_1 \\
&\bar{\sigma}_{21,1} + \bar{\sigma}_{22,2} + ik\bar{\sigma}_{23} + \alpha\xi^2\bar{\sigma}_{23,1} - \alpha\xi^1\bar{\sigma}_{23,2} + \alpha\bar{\sigma}_{31} = -\omega^2\rho\bar{u}_2 \\
&\bar{\sigma}_{31,1} + \bar{\sigma}_{32,2} + ik\bar{\sigma}_{33} + \alpha\xi^2\bar{\sigma}_{33,1} - \alpha\xi^1\bar{\sigma}_{33,2} = -\omega^2\rho\bar{u}_3
\end{aligned} \tag{38}$$

where $\bar{u}_i, \bar{\varepsilon}_{ij}, \bar{\sigma}_{ij}$ are complex components in the $\xi^1, \xi^2, \xi^3 (= x^3)$ directions.

In addition, traction-free boundary condition on $\partial\Omega$ is imposed, where $\partial\Omega$ is the lateral bounding surface of the beam and $\hat{n}$ is its normal vector:

$$\hat{\sigma}_{ij}\hat{n}_j = 0 \tag{39}$$

From strain-displacement relation, (28):

$$\hat{\varepsilon}_{11} = \hat{u}_{1,1}$$

$$\hat{\varepsilon}_{22} = \hat{u}_{2,2}$$

$$\hat{\varepsilon}_{33} = \hat{u}_{3,3} + \alpha\xi^2\hat{u}_{3,1} - \alpha\xi^1\hat{u}_{3,2}$$

$$2\hat{\varepsilon}_{23} = \hat{u}_{3,2} + \hat{u}_{2,3} + \alpha\xi^2\hat{u}_{2,1} - \alpha\xi^1\hat{u}_{2,2} + \alpha\hat{u}_1$$

$$2\hat{\varepsilon}_{13} = \hat{u}_{1,3} + \hat{u}_{3,1} + \alpha\xi^2\hat{u}_{1,1} - \alpha\xi^1\hat{u}_{1,2} - \alpha\hat{u}_2$$

$$2\hat{\varepsilon}_{12} = \hat{u}_{2,1} + \hat{u}_{1,2}$$

The strain-displacement relation for harmonic wave is obtained by substituding (37): $\hat{u}_i = \bar{u}_i e^{(\sqrt{-1}kx^3 - \sqrt{-1}\omega t)}$ into(28)

$$\left\{\hat{\varepsilon}\right\} = \begin{Bmatrix} \hat{\varepsilon}_{11} \\ \hat{\varepsilon}_{22} \\ \hat{\varepsilon}_{33} \\ 2\hat{\varepsilon}_{23} \\ 2\hat{\varepsilon}_{31} \\ 2\hat{\varepsilon}_{12} \end{Bmatrix} = \begin{Bmatrix} \bar{\varepsilon}_{11} \\ \bar{\varepsilon}_{22} \\ \bar{\varepsilon}_{33} \\ 2\bar{\varepsilon}_{23} \\ 2\bar{\varepsilon}_{31} \\ 2\bar{\varepsilon}_{12} \end{Bmatrix} e^{(\sqrt{-1}kx^3 - \sqrt{-1}\omega t)}$$

where $\bar{\varepsilon}_{ij}$, denotes the amplitude of strain components of harmonic wave, becomes:

$$\left\{\bar{\varepsilon}\right\} = \begin{Bmatrix} \bar{\varepsilon}_{11} \\ \bar{\varepsilon}_{22} \\ \bar{\varepsilon}_{33} \\ 2\bar{\varepsilon}_{23} \\ 2\bar{\varepsilon}_{31} \\ 2\bar{\varepsilon}_{12} \end{Bmatrix} = \begin{Bmatrix} \bar{u}_{1,1} \\ \bar{u}_{2,2} \\ ik\bar{u}_3 + \alpha\xi^2\bar{u}_{3,1} - \alpha\xi^1\bar{u}_{3,2} \\ \bar{u}_{3,2} + ik\bar{u}_2 + \alpha\xi^2\bar{u}_{2,1} - \alpha\xi^1\bar{u}_{2,2} + \alpha\bar{u}_1 \\ ik\bar{u}_1 + \bar{u}_{3,1} + \alpha\xi^2\bar{u}_{1,1} - \alpha\xi^1\bar{u}_{1,2} + \alpha\bar{u}_2 \\ \bar{u}_{2,1} + \bar{u}_{1,2} \end{Bmatrix} \tag{40}$$

The stress-strain relation is described by Hooke's law for isotropic material:

$$\left\{\bar{\sigma}\right\} = \begin{Bmatrix} \bar{\sigma}_{11} \\ \bar{\sigma}_{22} \\ \bar{\sigma}_{33} \\ \bar{\sigma}_{23} \\ \bar{\sigma}_{31} \\ \bar{\sigma}_{12} \end{Bmatrix} = \begin{bmatrix} \lambda+2\mu & \lambda & \lambda & 0 & 0 & 0 \\ \lambda & \lambda+2\mu & \lambda & 0 & 0 & 0 \\ \lambda & \lambda & \lambda+2\mu & 0 & 0 & 0 \\ 0 & 0 & 0 & \mu & 0 & 0 \\ 0 & 0 & 0 & 0 & \mu & 0 \\ 0 & 0 & 0 & 0 & 0 & \mu \end{bmatrix} \begin{Bmatrix} \bar{\varepsilon}_{11} \\ \bar{\varepsilon}_{22} \\ \bar{\varepsilon}_{33} \\ 2\bar{\varepsilon}_{23} \\ 2\bar{\varepsilon}_{31} \\ 2\bar{\varepsilon}_{12} \end{Bmatrix} \tag{41}$$

where λ and μ are Lame constants.

Equations of motion in terms of displacements are obtained by substituting (40) into (41) then into (38). The resulting equations define an eigenvalue problem for ω^2 when the wave number k is prescribed.

Since the eigenvalue problem defined on an arbitrary cross-section is not amenable for analytic solution, finite element method is employed to compute the ω versus k dispersion relation as well as the phase velocity spectra C_p versus k. The phase velocity is defined as

$$C_p = \frac{\omega}{k} \tag{42}$$

and group velocity is defined as

$$C_g = \frac{\partial \omega}{\partial k} \tag{43}$$

5 Finite Element Implementation

5.1 Principle of Virtual Work

For the harmonic wave form (37), the principle of virtual work (34) is reduced to over a cross-section A in the ξ^1, ξ^2 plane:

$$\int_A (\delta\bar{\varepsilon}_{ij}^* \bar{\sigma}_{ij} - \delta\bar{u}_i^* \rho\omega^2 \bar{u}_i + c.c) d\xi^1 d\xi^2 = 0 \tag{44}$$

where*indicates complex conjugate and "$c.c$" stands for complex conjugate terms. (Formulation from Murakami and Yamakawa 1998 [3])

5.2 Derivation of Stiffness Matrix

The cross-sectional domain A is divided into non-overlapping 4-node quadrilateral elements using isoparametric formulation. $A = \cup_{e=1}^{nel} A^{(e)}$

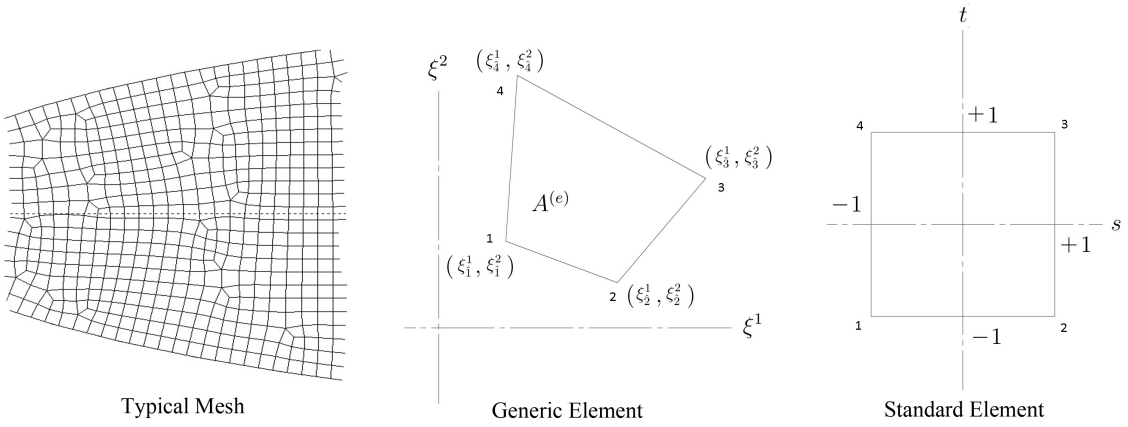

Figure 2: Iso-parametric Formulation

The shape functions in the standard domain $-1 \leq s \leq 1$, $-1 \leq t \leq 1$ are:

$$\begin{aligned} N_1 &= \frac{(1-s)(1-t)}{4} \qquad N_2 = \frac{(1+s)(1-t)}{4} \\ N_3 &= \frac{(1+s)(1+t)}{4} \qquad N_4 = \frac{(1-s)(1+t)}{4} \end{aligned} \tag{45}$$

The coordinate mapping between the standard element and a generic element is defined by using the nodal coordinates $\xi_{\hat{i}}^1, \xi_{\hat{i}}^2$ (where node number $i = 1, 2, 3, 4$) of

the element in the ξ^1, ξ^2 domain as follows:

$$\begin{Bmatrix} \xi^1 \\ \xi^2 \end{Bmatrix} = \begin{Bmatrix} N_1 & N_2 & N_3 & N_4 & 0 & 0 & 0 & 0 \\ 0 & 0 & 0 & 0 & N_1 & N_2 & N_3 & N_4 \end{Bmatrix} \begin{Bmatrix} \xi^1_{\hat{1}} \\ \xi^1_{\hat{2}} \\ \xi^1_{\hat{3}} \\ \xi^1_{\hat{4}} \\ \xi^2_{\hat{1}} \\ \xi^2_{\hat{2}} \\ \xi^2_{\hat{3}} \\ \xi^2_{\hat{4}} \end{Bmatrix} \tag{46}$$

Displacements are interpolated by using nodal displacement values $\bar{v}_k^{\hat{j}}$ where $j = 1, 2, 3, 4$ denotes element node number and $k = 1, 2, 3$.

$$\begin{Bmatrix} \bar{u}_1 \\ \bar{u}_2 \\ \bar{u}_3 \end{Bmatrix} = \sum_{j=1}^{4} \begin{bmatrix} N_j & 0 & 0 \\ 0 & N_j & 0 \\ 0 & 0 & N_j \end{bmatrix} \begin{Bmatrix} \bar{v}_1^{\hat{j}} \\ \bar{v}_2^{\hat{j}} \\ \bar{v}_3^{\hat{j}} \end{Bmatrix} \tag{47}$$

Substituting (47) into (40), the strain - (nodal) displacement relation is obtained.

$$\left\{ \bar{\varepsilon} \right\}^{(e)} = \sum_{j=1}^{4} \left[B_j \right]^{(e)} \begin{Bmatrix} \bar{v}_1^{\hat{j}} \\ \bar{v}_2^{\hat{j}} \\ \bar{v}_3^{\hat{j}} \end{Bmatrix}^{(e)}$$

$$\Big[B_j\Big]^{(e)} = \begin{bmatrix} N_{j,1} & 0 & 0 \\ 0 & N_{j,2} & 0 \\ 0 & 0 & ikN_j + \alpha\xi^2 N_{j,1} - \alpha\xi^1 N_{j,2} \\ \alpha N_j & ikN_j + \alpha\xi^2 N_{j,1} - \alpha\xi^1 N_{j,2} & N_{j,2} \\ ikN_j + \alpha\xi^2 N_{j,1} - \alpha\xi^1 N_{j,2} & -\alpha N_j & N_{j,1} \\ N_{j,2} & N_{j,1} & 0 \end{bmatrix} \tag{48}$$

In (48), $N_{j,i} = \frac{\partial N_j}{\partial \xi^i}$, $i = 1, 2$, referred to as cartesian derivative of shape functions and they are defined as:

$$\begin{Bmatrix} N_{j,1} \\ N_{j,2} \end{Bmatrix} = \frac{1}{|J|} \begin{bmatrix} \frac{\partial \xi^2}{\partial t} & -\frac{\partial \xi^2}{\partial s} \\ -\frac{\partial \xi^1}{\partial t} & \frac{\partial \xi^1}{\partial s} \end{bmatrix} \begin{Bmatrix} \frac{\partial N_j}{\partial s} \\ \frac{\partial N_j}{\partial t} \end{Bmatrix} \tag{49}$$

$$|J| = \begin{vmatrix} \frac{\partial \xi^1}{\partial s} & \frac{\partial \xi^2}{\partial s} \\ \frac{\partial \xi^1}{\partial t} & \frac{\partial \xi^2}{\partial t} \end{vmatrix} \tag{50}$$

The virtual strain energy term is then written using (41) and (48) as:

$$\int_A \delta\bar{\varepsilon}^*_{ij}\bar{\sigma}_{ij} d\xi^1 d\xi^2 = \sum_{e=1}^{nel} \int_{A(e)} \Big\{\delta\bar{v}\Big\}^{*T(e)} \Big[B\Big]^{*T(e)} \Big[D\Big] \Big[B\Big] \Big\{\bar{v}\Big\}^{(e)} d\xi^1 d\xi^2 \tag{51}$$

where

$$\Big\{\bar{\sigma}\Big\} = \Big[D\Big] \Big\{\bar{\varepsilon}\Big\}$$

Element stiffness matrix derived from virtual strain energy is then obtained

by using 9 Gauss integration points over the standard domain as follows:

$$\left[K\right]^{(e)} = \int_{-1}^{1}\int_{-1}^{1} \left[B\right]^{*T^{(e)}} \left[D\right]^{(e)} \left[B\right]^{(e)} |J|^{(e)} ds dt \tag{52}$$

5.3 Derivation of Mass Matrix

The principle of virtual work (44) indicates that element mass matrix can be derived from expression:

$$\int_A \delta\bar{u}_i^* \rho\omega^2 \bar{u}_i d\xi^1 d\xi^2 = \sum_{e=1}^{nel} \int_{A(e)} \delta\bar{u}_i^* \rho\omega^2 \bar{u}_i d\xi^1 d\xi^2 \tag{53}$$

The displacement field is interpolated by using nodal values as described in (47), the expanded form can be expressed as:

$$\begin{Bmatrix} \bar{u}_1 \\ \bar{u}_2 \\ \bar{u}_3 \end{Bmatrix} = [N] \left\{\bar{v}\right\}^{(e)} \tag{54}$$

where

$$[N] = \begin{bmatrix} N_1 & 0 & 0 & N_2 & 0 & 0 & N_3 & 0 & 0 & N_4 & 0 & 0 \\ 0 & N_1 & 0 & 0 & N_2 & 0 & 0 & N_3 & 0 & 0 & N_4 & 0 \\ 0 & 0 & N_1 & 0 & 0 & N_2 & 0 & 0 & N_3 & 0 & 0 & N_4 \end{bmatrix} \tag{55}$$

$$\left\{\bar{v}\right\}^{(e)} = \begin{Bmatrix} \bar{v}_1^{\hat{1}} & \bar{v}_2^{\hat{1}} & \bar{v}_3^{\hat{1}} & \bar{v}_1^{\hat{2}} & \bar{v}_2^{\hat{2}} & \bar{v}_3^{\hat{2}} & \bar{v}_1^{\hat{3}} & \bar{v}_2^{\hat{3}} & \bar{v}_3^{\hat{3}} & \bar{v}_1^{\hat{4}} & \bar{v}_2^{\hat{4}} & \bar{v}_3^{\hat{4}} \end{Bmatrix}^T \tag{56}$$

Substitute (54) into (53):

$$\int_A \delta\bar{u}_i^* \rho\omega^2 \bar{u}_i d\xi^1 d\xi^2 = \sum_{e=1}^{nel} \omega^2 \int_{A(e)} \left\{\bar{v}\right\}^{*T(e)} \left[N\right]^T \rho \left[N\right] \left\{\bar{v}\right\}^{(e)} d\xi^1 d\xi^2 \tag{57}$$

Mass matrix is then given by:

$$\left[M\right]^{(e)} = \rho \int_{-1}^{1} \int_{-1}^{1} [N]^T [N] |J|^{(e)} ds dt \tag{58}$$

The principle of virtual work is now written as:

$$\sum_{e=1}^{e=nel} \left\{\delta\bar{v}^*\right\}^{T(e)} [K]^{(e)} \left\{\bar{v}\right\}^{(e)} = \omega^2 \sum_{e=1}^{e=nel} \left\{\delta\bar{v}^*\right\}^{T(e)} [M]^{(e)} \left\{\bar{v}\right\}^{(e)} \tag{59}$$

Finally, assemble the above for arbitrary variational displacements to find a generalized eigenvalue problem:

$$\left\{\delta\bar{v}^*\right\} : \left[K\right] \left\{\bar{v}\right\} = \omega^2 \left[M\right] \left\{\bar{v}\right\} \tag{60}$$

where $\left[K\right]$ is Hermitian

$$\left[K\right]^{*T} = \left[K\right]$$

and $\left[M\right]$ is symmetric

$$\left[M\right]^{T} = \left[M\right]$$

The generalized eigenvalue problem with hermitian matrices are proven to have real eigen values and $\left[K\right]$ and $\left[M\right]$ are diagonalizable.

The finite element code was developed to solve the above genrealized eigen

value problem utilizing the inverse iteration method (Bathe [16], 1982). The following section presents the numerical results.

6 Numerical Results

In this section, numerical results of dispersion relation of harmonic waves in straight and pre-twisted beams are presented for two rectangular cross-sections and one elliptic cross-section. The objective is to investigate the effect of pre-twist on phase velocity spectra and corresponding mode shapes.

6.1 Cross-sectional Geometry

For this numerical analysis, rectangular and elliptic cross-sections are considered.

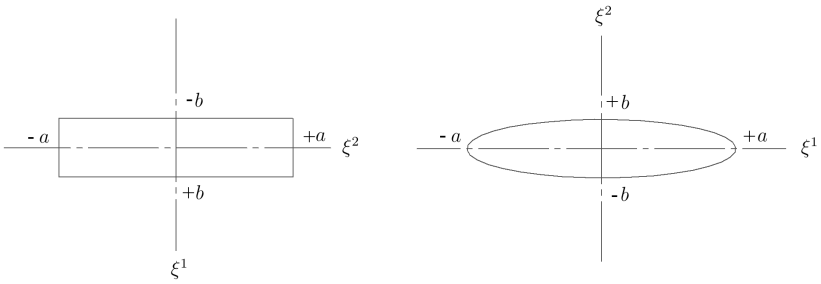

Figure 3: Rectangular and Elliptic Cross-sections

The geometry of these cross-sections are described in Table 1

The finite element mesh used for rectangular cross-sections with aspect ratios of 4:1 and 2:1 are obtained by uniformly diving the cross-section into 200x50 and

	Cross-section (i)	Cross-section (ii)	Cross-section (iii)
Geometry	Rectangular	Rectangular	Elliptic
$2a$	0.2m	0.1m	0.25m
$2b$	0.05m	0.05m	0.05
a/b	4:1	2:1	5:1

Table 1: Geometry of Cross-sections

100x50 elements respectively. The mesh used for the elliptic crosss section is shown in Figure 4 and Figure 5, and it is generated by AutoMesh2D.

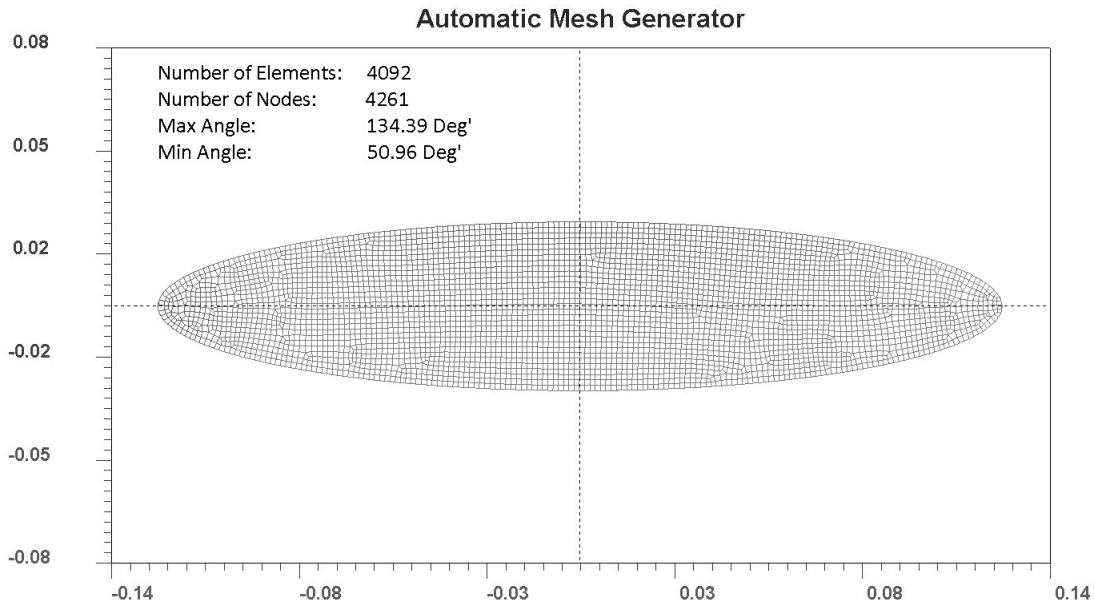

Figure 4: Elliptic Cross-Section Mesh in ξ^1,ξ^2 Plane - View 1

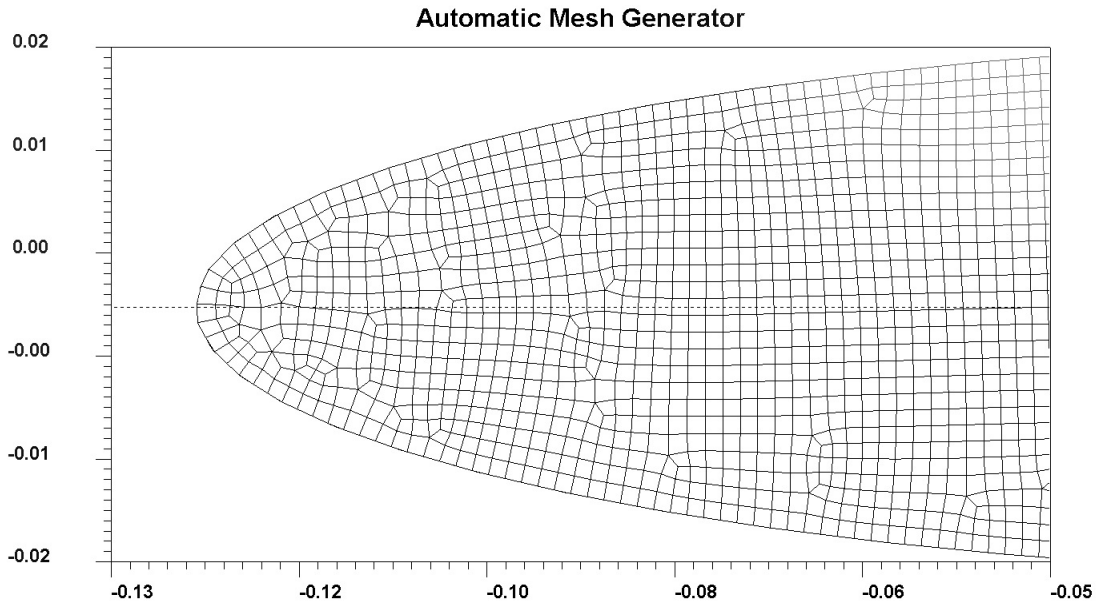

Figure 5: Elliptic Cross-Section Mesh in ξ^1,ξ^2 Plane - View 2

Material Properties:

E = 69 Gpa G = 24 Gpa $\rho = 7874\ kg/m^3$

(6061 Aluminum alloy)

Bar velocity is defined as: $C_o = \sqrt{\frac{E}{\rho}}$

6.2 Phase Velocity Spectra and the Effect of Pretwist

In order to clarify the effect of pre-twist angle, dispersion spectra were computed for straight beam, $45^o/m$ pre-twist and $90^o/m$ pre-twist for each cross-section defined in Table 1.

For the rectangular cross-section with the larger aspect ratio 4:1, the dispersion spectra, ω versus k curves, are plotted in Figure 6 and the corresponding phase velocity spectra, C_p versus k curves, are shown in Figure 8. These figures show

four lowest modes consisting of longitudinal, torsional, bending with minor axis,and bending with major axis.

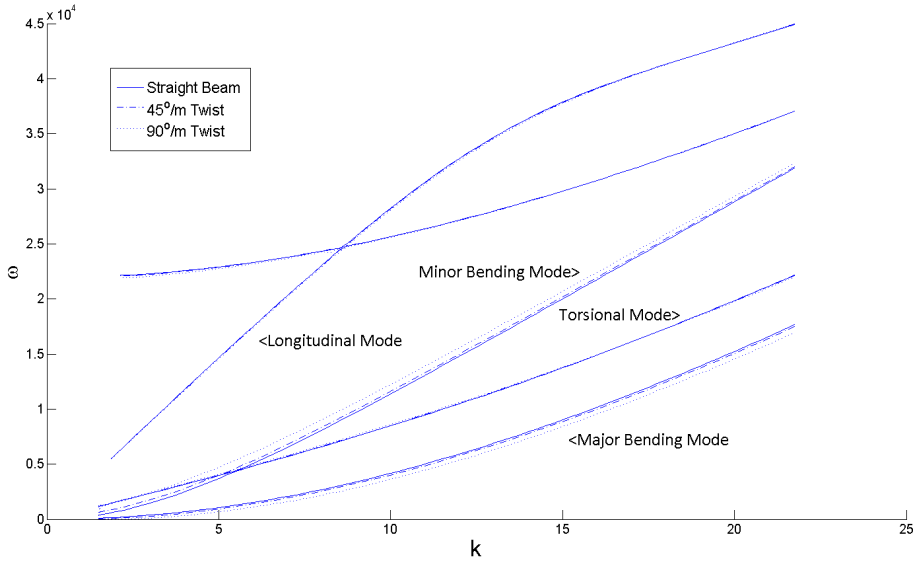

Figure 6: Effect of Twist Angle on Wave Dispersion of Rectangular Beam with Aspect Ratio of 4:1 (ω vs k)

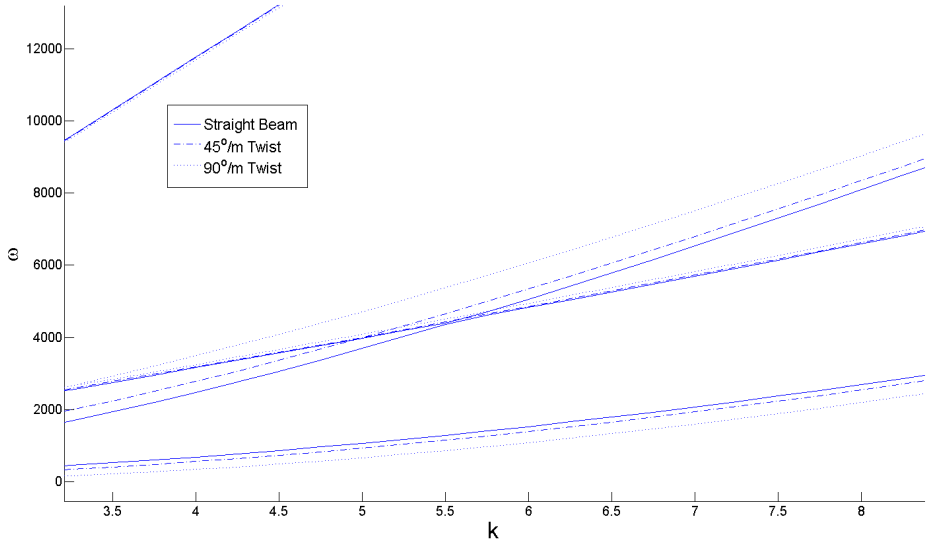

Figure 7: Close-up View of Figure 6

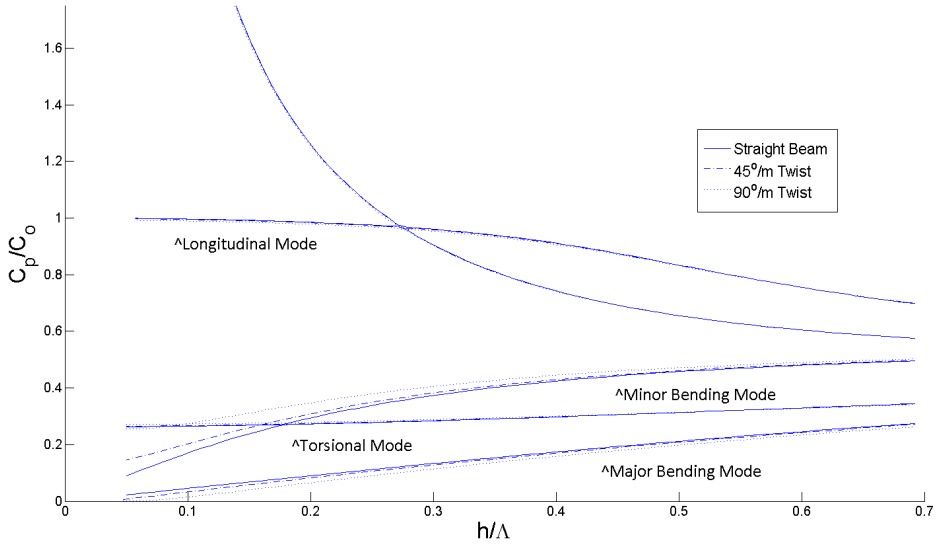

Figure 8: Effect of Twist Angle on Phase Velocity of Rectangular Beam with Aspect Ratio of 4:1 ($\frac{C_p}{C_o}$ vs $\frac{h}{\Lambda}$)

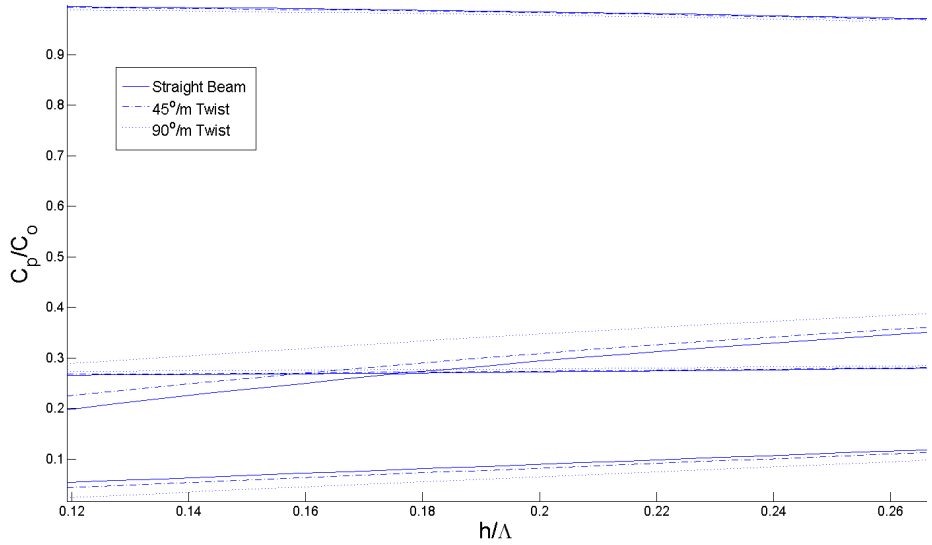

Figure 9: Close-up View of Figure 8

Figure 8 shows that longitudinal mode exhibits dispersion at higher wave number, similar to the dispersion of rod with circular cross-section, known as the Pochhammer-Chree dispersion relation. The effect of pre-twist on the longitudinal mode is minute but noticeable. The torsional mode exhibits negligible dispersion and minute effect of pre-twist.

On the contrary, bending modes showed pronounced dispersion and the effect of pretwist. The dispersion spectra of pre-twisted beams exhibit the same trend as that of straight beams, only they are shifted. The phase velocity of the minor bending mode increases due to pre-twist, while that of the major bending reduces due to pre-twist. This trend agrees with the static analysis of bending stiffness of pre-twisted beams by Goodier and Griffin [5] (1969), interpreting that higher bending phase velocity translates to higher bending stiffness. However, their semi-inverse analysis only applies to small pre-twist angles since they used the asymptotic expansion with respect to small pre-twist angle and kept only the first term.

Dispersion spectra of the beams with rectangular cross-section with smaller aspect ratio 2:1 is shown in Figure 10 , and the corresponding phase velocity spectra are plotted in Figure 12.

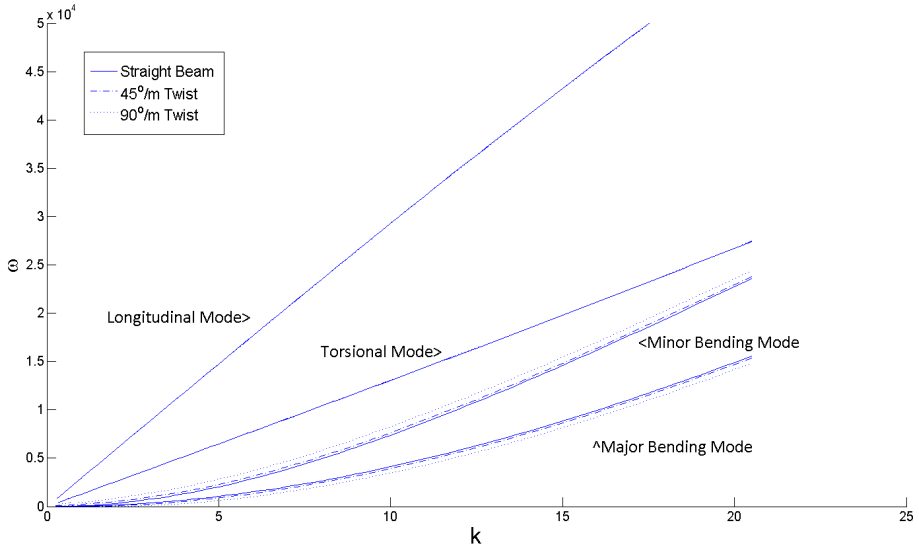

Figure 10: Effect of Twist Angle on Wave Dispersion of Rectangular Beam with Aspect Ratio of 2:1 (ω vs k)

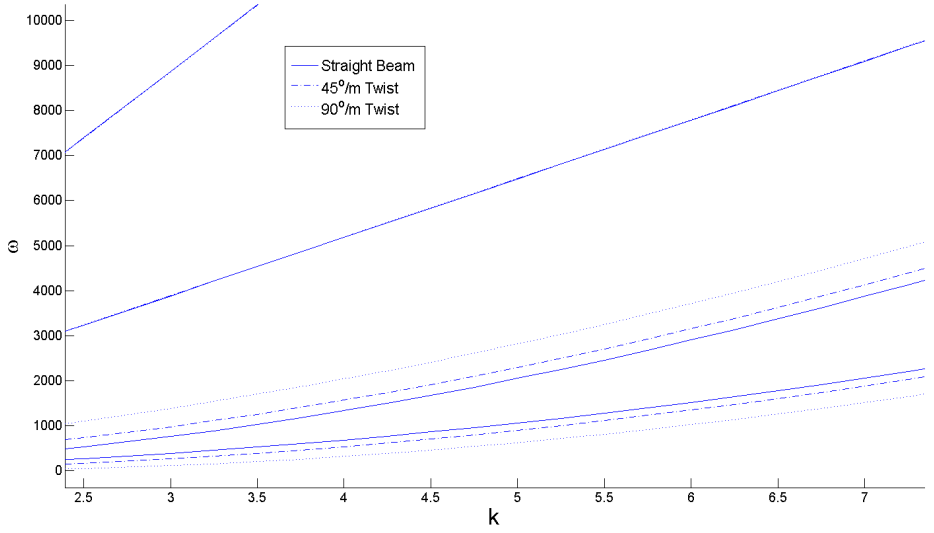

Figure 11: Close-up View of Figure 10

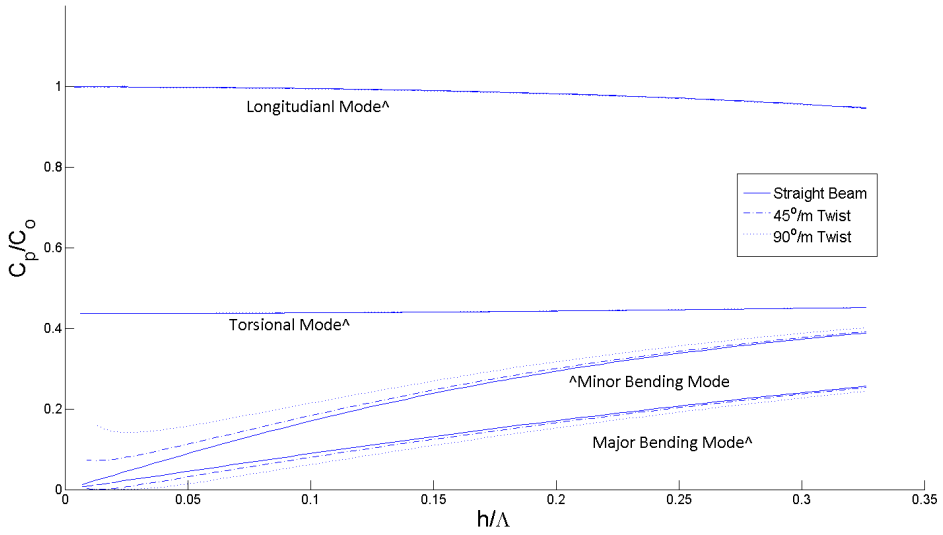

Figure 12: Effect of Twist Angle on Phase Velocity of Rectangular Beam with Aspect Ratio of 2:1 ($\frac{C_p}{C_o}$ vs $\frac{h}{\Lambda}$)

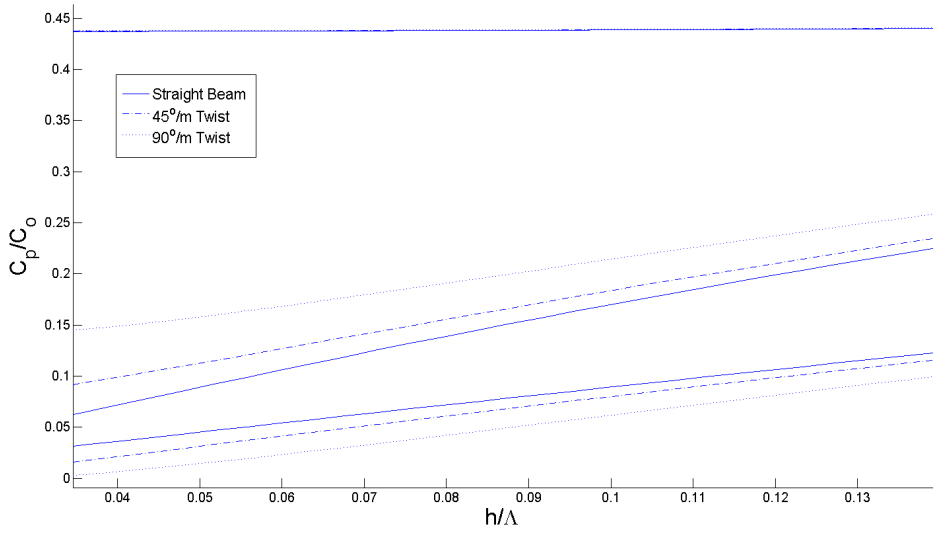

Figure 13: Close-up View of Figure 12

In Figure 12, the torsional phase velocity of the cross-section with aspect ratio 2:1 is larger than that of the cross-section with aspect ratio 4:1 shown in Figure 8 since the torsional stiffness increases for the cross-section with smaller aspect ratio. The effect of pre-twist is observed to be even less siginificant for both longitudinal and torsional modes than previously discussed rectangular cross-sections with aspect ratio of 4:1.

In the bending modes the effect of pre-twist shift the phase velocity spectra with the same trend as that of the cross-section with larger aspect ratio 4:1. The phase velocity of the minor bending modes increases as the pre-twist angle increases. On the contrary, the phase velocity of the major bending modes decreases as the pre-twist angle increases.

The dispersion spectra for the elliptic cross-section is shown in Figure 14, and the phase velocity spectra are presented in Figure 16.

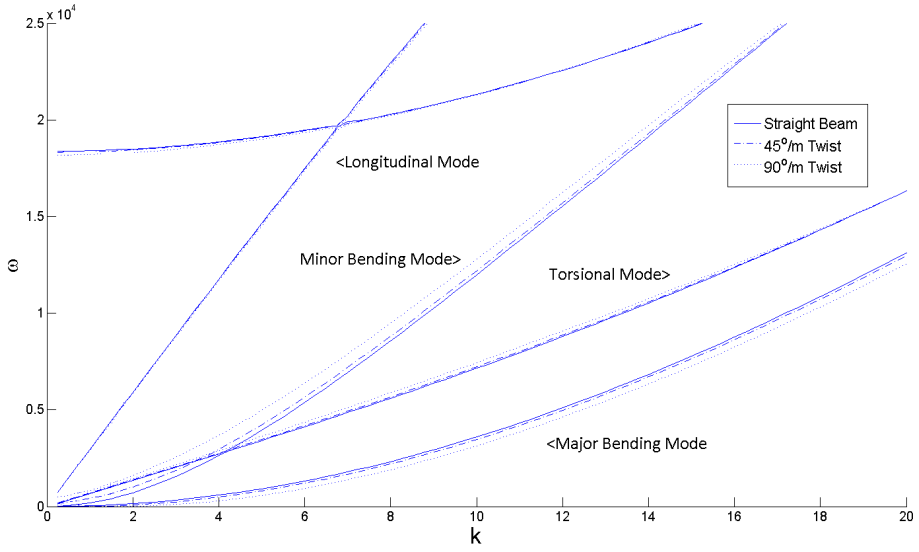

Figure 14: Effect of Twist Angle on Wave Dispersion of Elliptic Beam with Aspect Ratio of 5:1 (ω vs k)

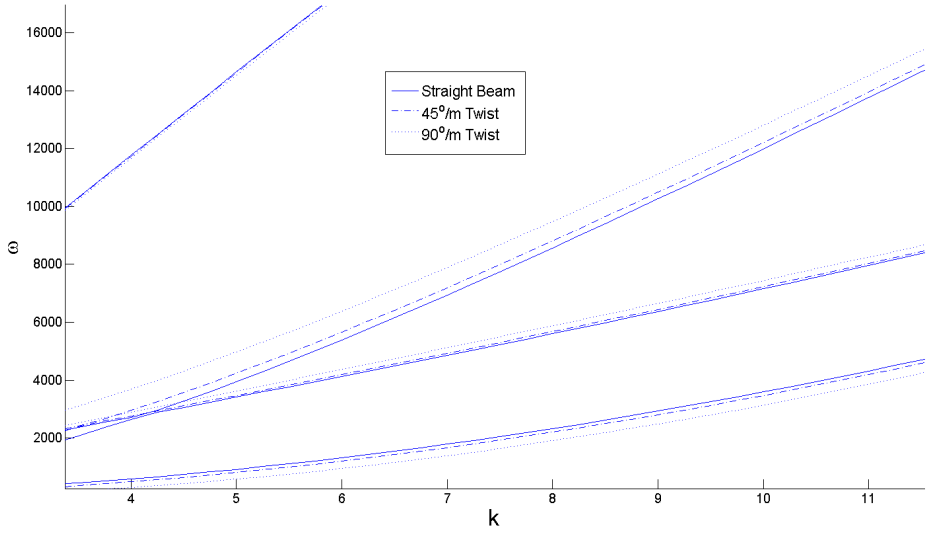

Figure 15: Close-up View of Figure 14

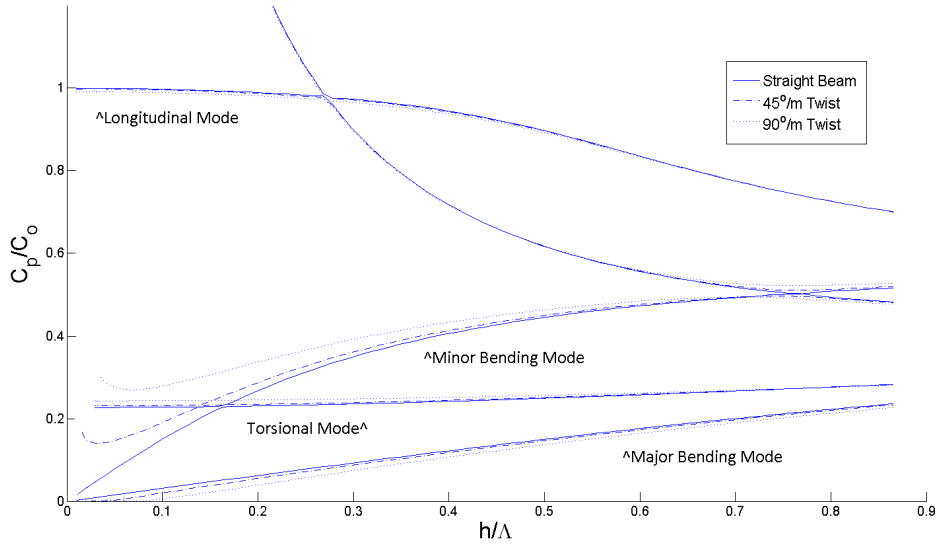

Figure 16: Effect of Twist Angle on Phase Velocity of Elliptic Beam with Aspect Ratio of 5:1 ($\frac{C_p}{C_o}$ vs $\frac{h}{\Lambda}$)

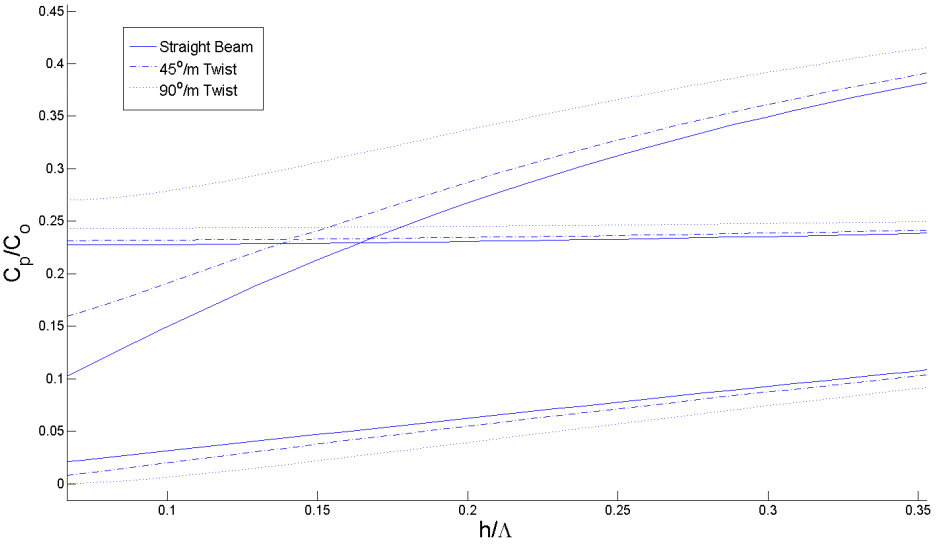

Figure 17: Close-up View of Figure 16

Similar to the previous two cases, the velocity of the minor bending modes increases as the pre-twist angle increases and the phase velocity of the major bending modes decreases as the pre-twist angle increases. The pre-twist effect on longitudinal and torsional modes are more significant for this case. Judging by the trend, it is presumably due to higher aspect ratio.

6.3 Mode Shape Interpretation and the Effect of Pre-twist

In this section, modes shapes of harmonic waves in the pre-twist beams and the straight beams are presented. Since mode shapes of the lowest four modes for three cross-sections, shown in Table 1.1, are similar, only the mode shapes for the 4:1 aspect ratio rectangular cross-section with pre-twist rate of $45^o/m$ are presented in the following at the wave number $k = 7$ or $h/\Lambda = 0.22$.

To show the effect of pre-twist on mode shapes, modes of the pre-twisted beam is compared to the modes of the straight beams with the same cross-section whenever appropriate. In the subsequent figures, when the modes of pre-twist and straight beams are plotted in the same figure, the boundary of the cross-section of the pre-twisted beam is highlighted by red border lines.

In plotting the mode shape, it is noted that the generalized eigenvalue problem defined by (60) gives complex amplitude, $\bar{u}$, of harmonically traveling waves. The displacements are described by: $[(\bar{u}_i)_{real} + \sqrt{-1}(\bar{u}_i)_{imaginary}][cos(kx^3 - wt) + \sqrt{-1}sin(kx^3 - wt)]$ (Euler's formula). Simplifying and evaluating only the real part, the following expression for displacement is obtained: $(\bar{u}_i)_{real}cos(kx^3 - wt) - (\bar{u}_i)_{imaginary}sin(kx^3 - wt)$.

As time progresses at fixed x^3, $cos(kx^3-wt)$and $sin(kx^3-wt)$ cycles from -1 to 1. If frame is taken every quarter of a period, the mode shapes can be represented by 4 chronologically consecutive frames described by displacements: $(+\bar{u}_i)_{imaginary}$,$(+\bar{u}_i)_{real}$, $(-\bar{u}_i)_{imaginary}$, $(-\bar{u}_i)_{real}$ in that order, which correspond to phase angle 0^o, 90^o, 180^o and 270^o.

In addition, to highlight the x^3 displacement of the modes, the color scale shown in Figure 18 is employed.

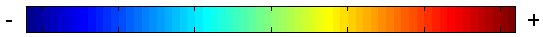

Figure 18: x^3 Displacement Color Scale

where it's scaled from the lowest to highest x^3 displacement of the corresponding mode shape.

Mesh as seen in the figures does not represent element boundary. To reduce clutter, it is the outline of the boundaries between every 5 elements.

6.3.1 Longitudinal Modes

Longitudinal modes exhibit translation of the cross-sections in the x^3 direction for both pre-twisted and straight beams. Figures 19-22 illustrate the x^3 positions of the cross-sections viewed in the direction of the minor axis at phase angle 0^o, 90^o, 180^o, and 270^o, respectively. The modes show warping of the cross-sections to satisfy lateral traction free condition.

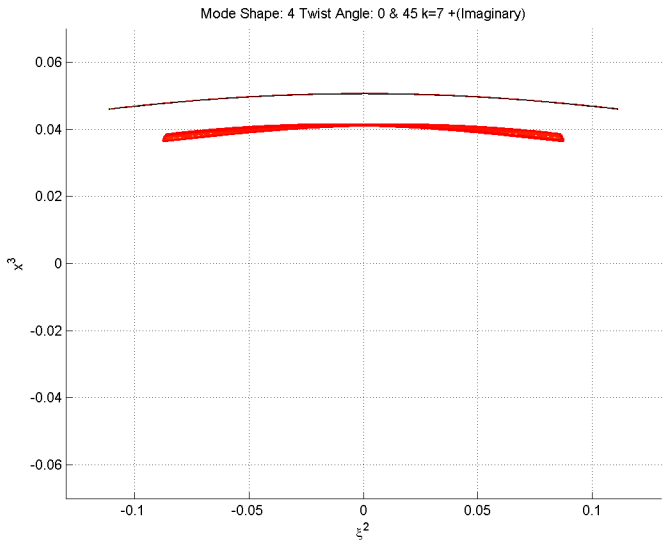

Figure 19: Mode 4 - 45^o Twist Overlay Top View +Imaginary

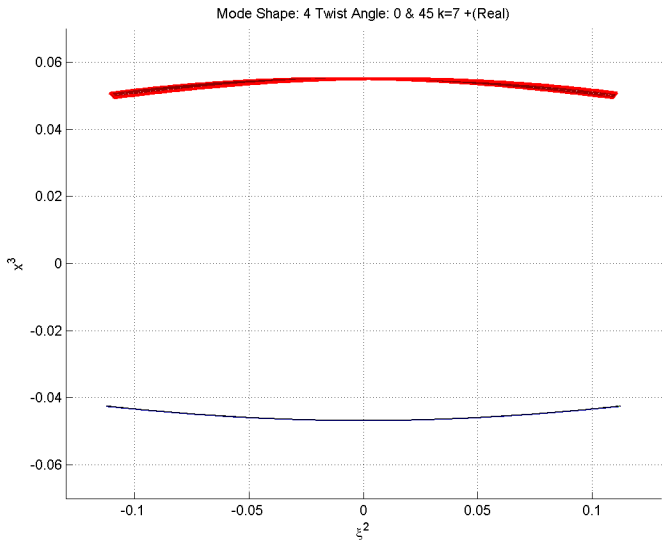

Figure 20: Mode 4 - 45^o Twist Overlay Top View +Real

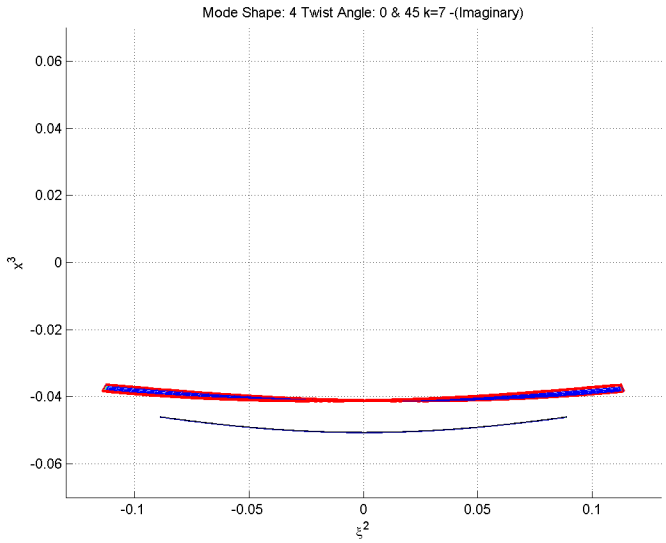

Figure 21: Mode 4 - 45^o Twist Overlay Top View -Imaginary

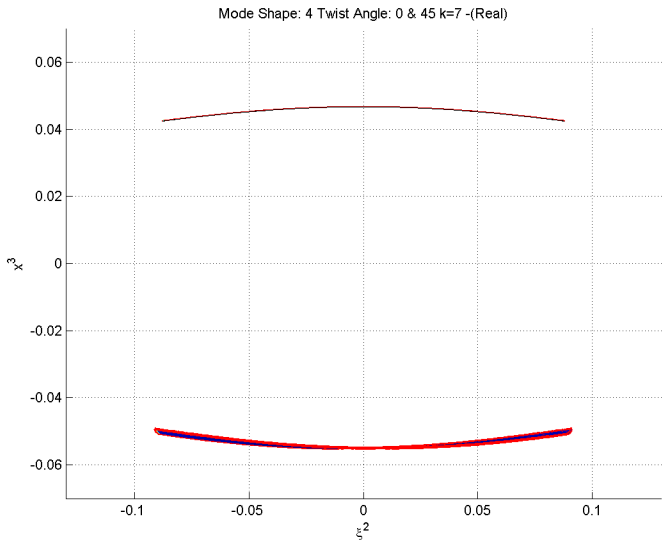

Figure 22: Mode 4 - 45^o Twist Overlay Top View -Real

Figures 23-26 illustrate the longitudinal modes projected on the ξ^1, ξ^2 plane. In the figures, straight beam cross-section exhibits Poisson's contraction of cross-section without any rotation of the cross-section. On the other hand, the cross-section of pre-twisted beam rocks with respect to the x^3 axis indicating that torsional deformation appears with longitudinal deformation.

Therefore, the gross longitudinal mode of the pre-twisted beam includes the coupling of longitudinal and torsional deformations. While the longitudinal mode of the straight beam exhibits purely longitudinal.

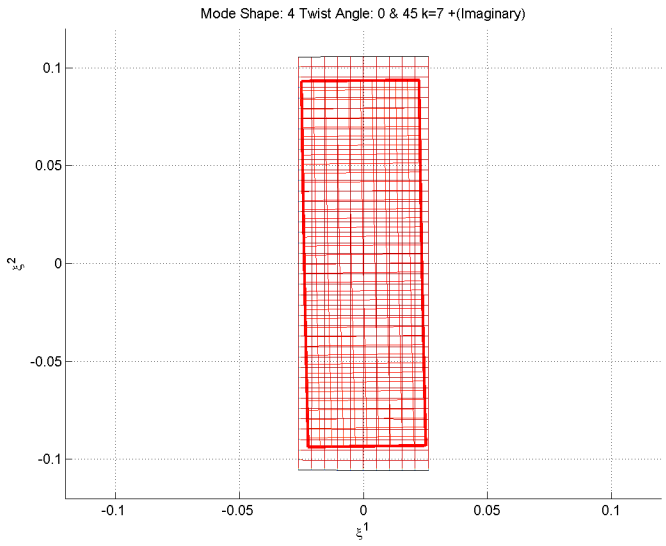

Figure 23: Mode 4 - 45^o Twist Overlay Top View +Imaginary

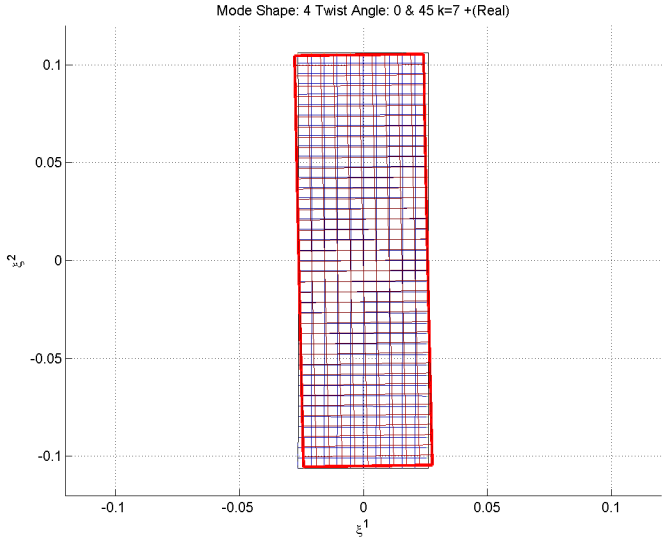

Figure 24: Mode 4 - 45^o Twist Overlay Top View +Real

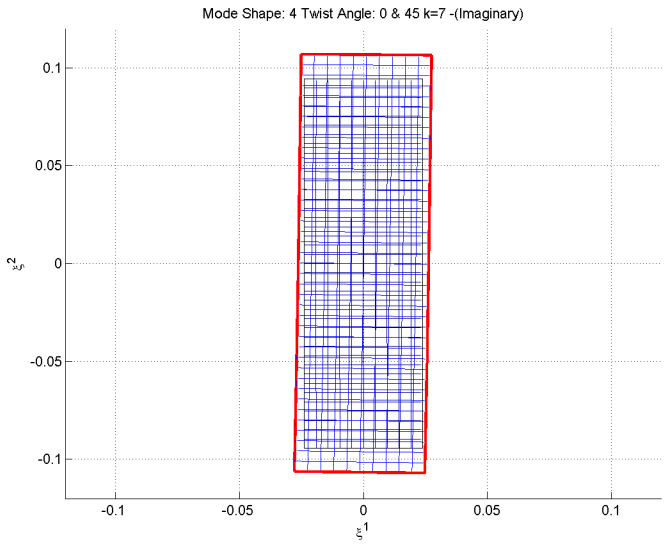

Figure 25: Mode 4 - 45^o Twist Overlay Top View -Imaginary

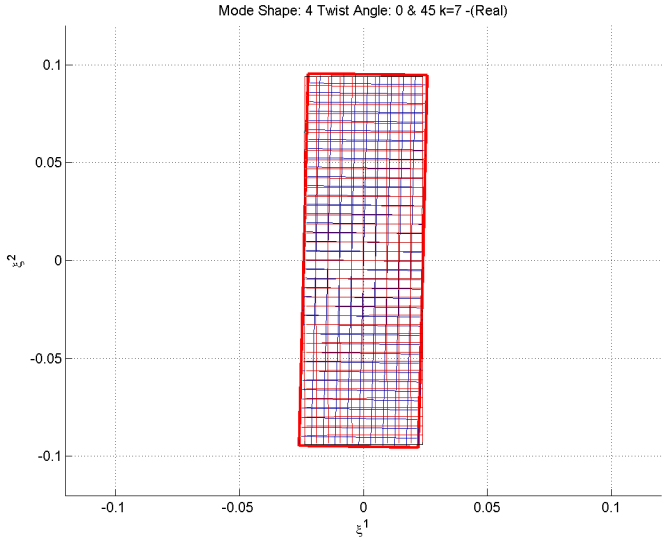

Figure 26: Mode 4 - 45^o Twist Overlay Top View -Real

6.3.2 Torsional Modes

Torsional modes exhibit rocking of the cross-section (in the ξ^1, ξ^2 plane), about the x^3 axis, which are presented in Figures 27-30 (Only showing cross-section for 45^o pre-twist). The modes of the pre-twisted and straight beams are similar to each other in this regard.

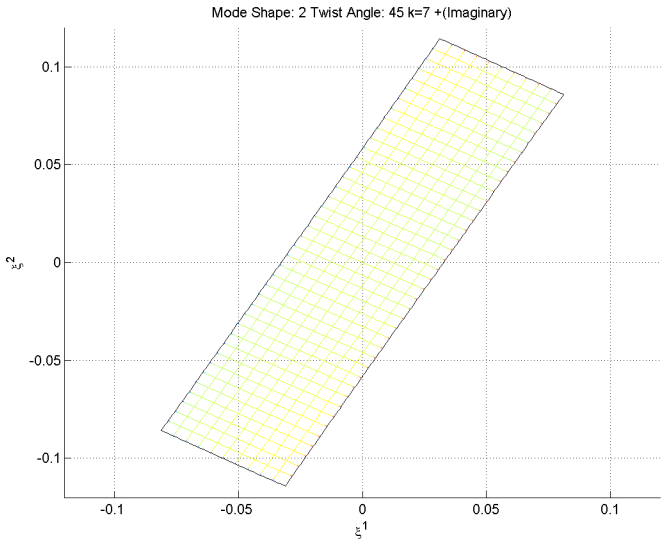

Figure 27: Mode 2 - 45^o Twist Top View (+Imaginary)

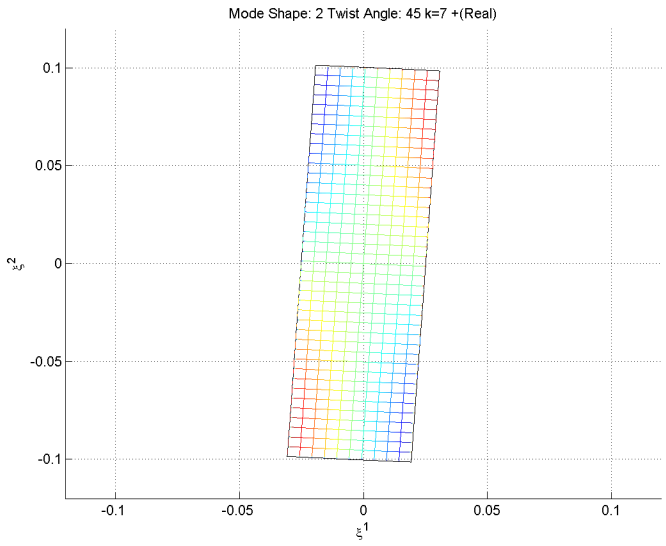

Figure 28: Mode 2 - 45^o Twist Top View (+Real)

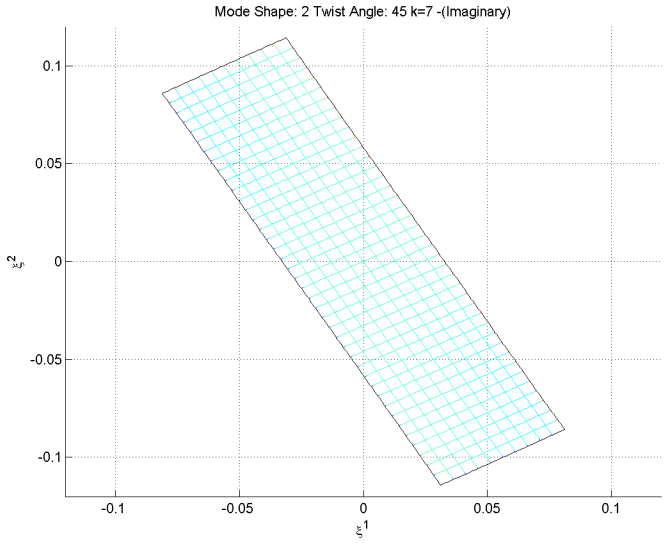

Figure 29: Mode 2 - 45^o Twist Top View (-Imaginary)

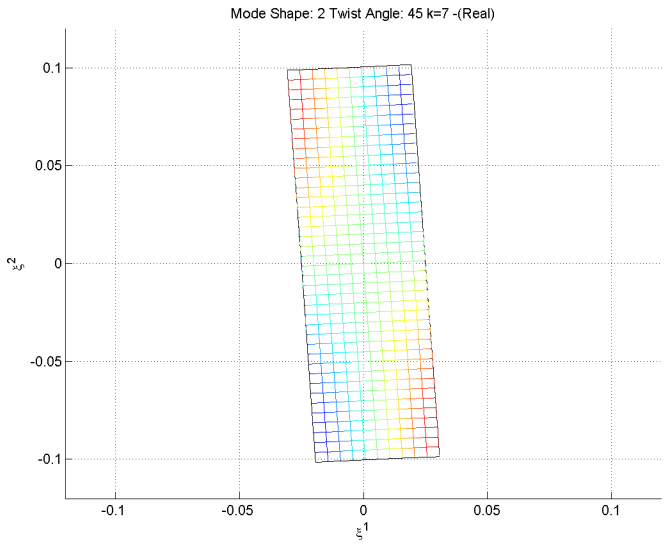

Figure 30: Mode 2 - 45^o Twist Top View (-Real)

Figures 31-34 shows the x^3-displacement of the modes viewed along the minor axis of the cross-section. The center of the cross-section of the straight beam does not translate in the x^3-direction, but the cross-section shows warping. The red border lines of the cross-section of the pre-twisted beam show the x^3-translation in addition to the warping of the cross-section. This is the coupling of torsional and longitudinal deformations in the pre-twisted beam, consistent with the Betti-Rayleight reciprocity principle (for example, Fung and Tong [1], 2001).

This coupling of torsional and longitudinal deformations is the unique feature of pre-twisted beams, which does not exist in straight beams.

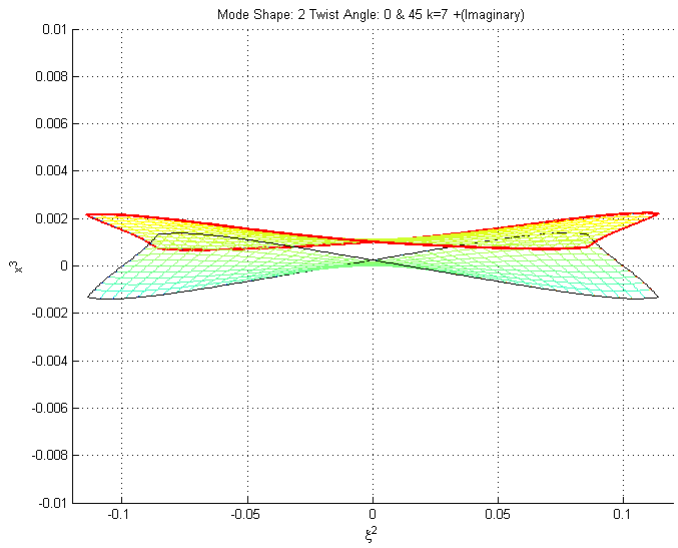

Figure 31: Mode 2 - 45^o Twist Overlay Side View (+Imaginary) Re-scaled x^3 axis

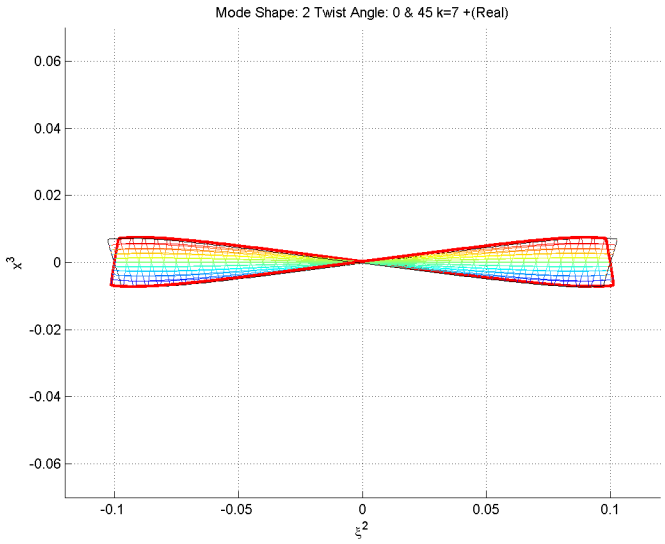

Figure 32: Mode 2 - 45^o Twist Overlay Side View (+Real)

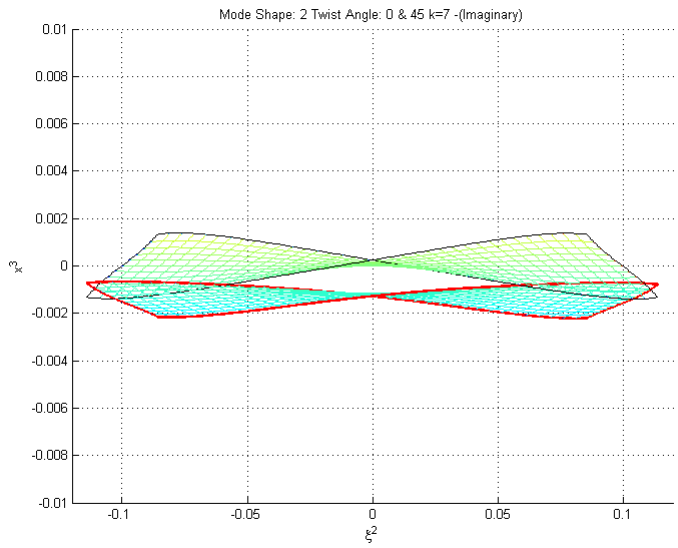

Figure 33: Mode 2 - 45^o Twist Overlay Side View (-Imaginary) Re-scaled x^3 axis

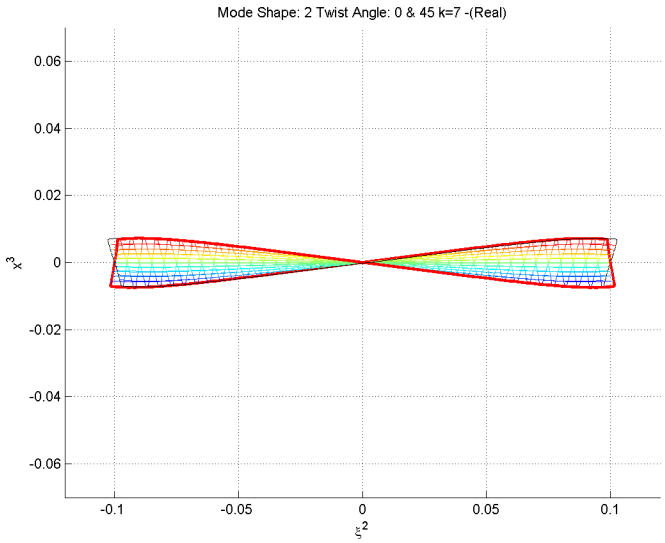

Figure 34: Mode 2 - 45^o Twist Overlay Side View (-Real)

6.3.3 Bending Modes with respect to Minor Axis (ξ^1):

Figures 35-38 illustrate the bending modes with respect to minor axis projected on to the ξ^1, ξ^2 -plane. The modes illustrate the translational displacement along the major axis. The modes of the pre-twisted beam show the translation in the minor axis direction due to the effect of pre-twist.

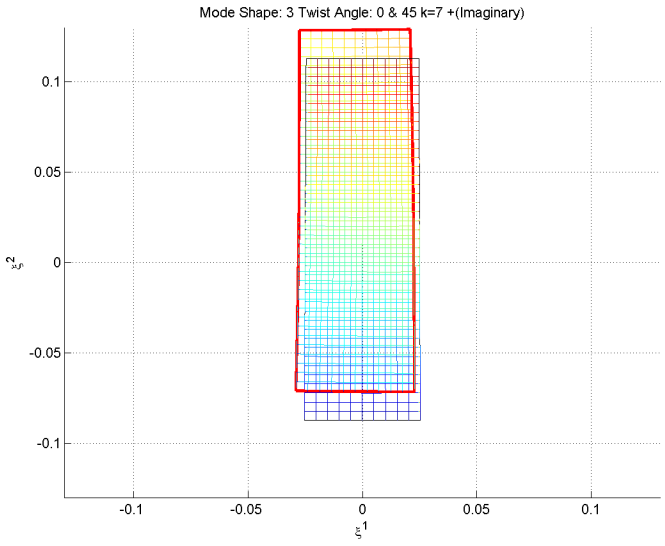

Figure 35: Mode 3 - 45^o Twist Overlay Top View +Imaginary

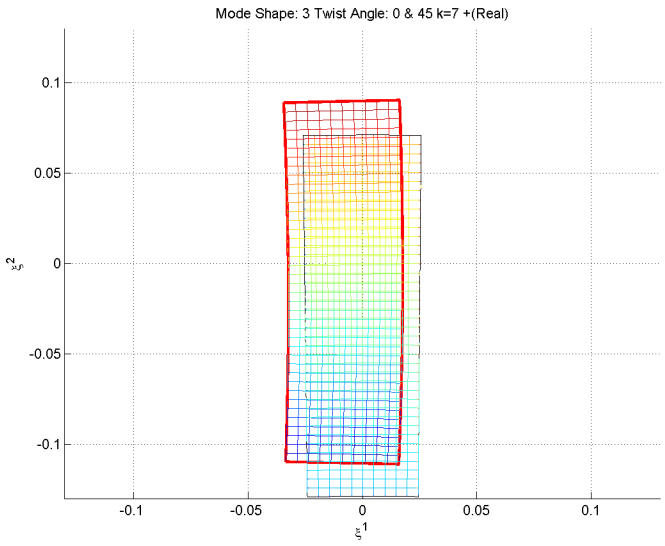

Figure 36: Mode 3 - 45^o Twist Overlay Top View +Real

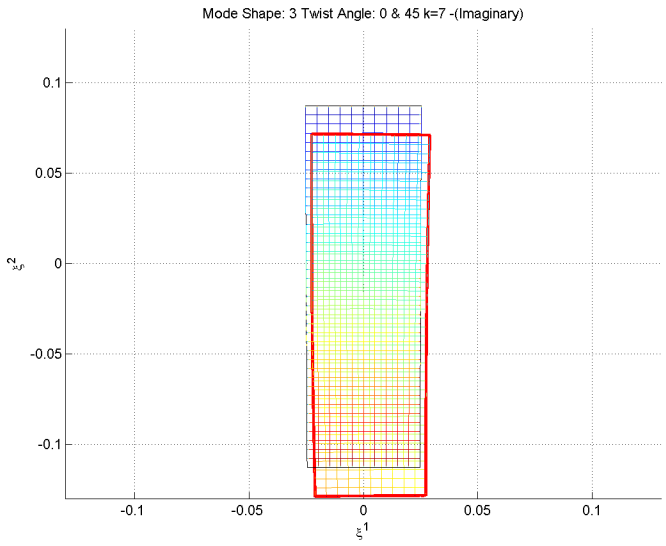

Figure 37: Mode 3 - 45^o Twist Overlay Top View -Imaginary

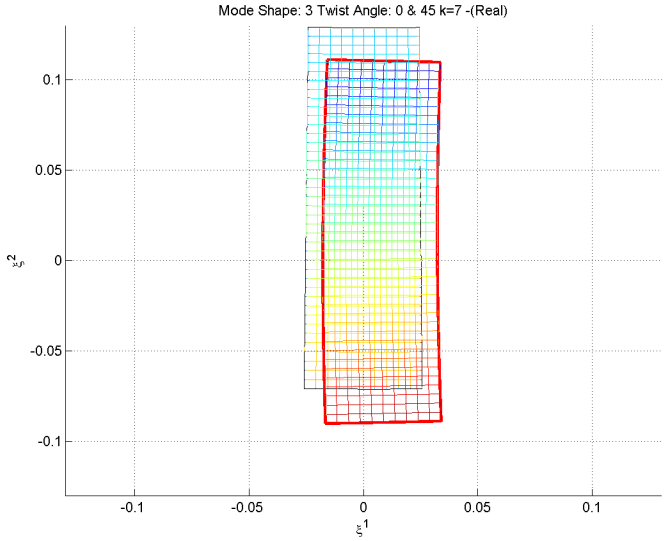

Figure 38: Mode 3 - 45^o Twist Overlay Top View -Real

The projections of the cross-sections onto the ξ^2, x^3 -plane are shown in Figures 39-42. The figures illustrate the typical bending deformation of the cross-sections in

which the corss-section rocks with respect to the minor axis. The cross-section of the pre-twisted beam exhibits minute rocking with respect to the major axis.

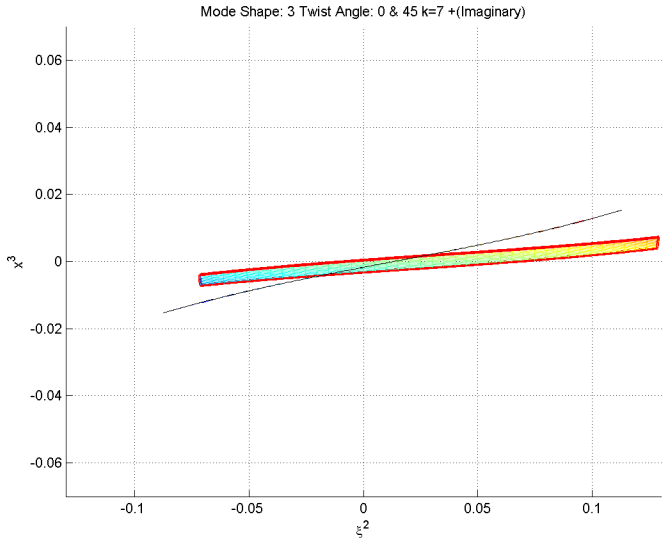

Figure 39: Mode 3 - 45^o Twist Overlay Side View +Imaginary

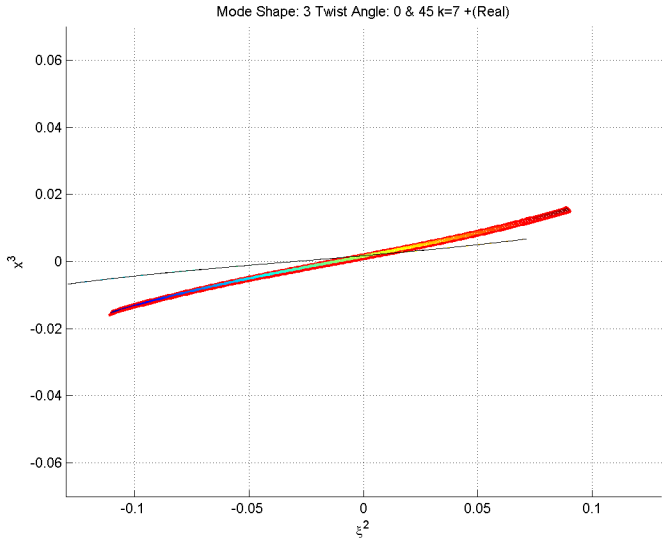

Figure 40: Mode 3 - 45^o Twist Overlay Side View +Real

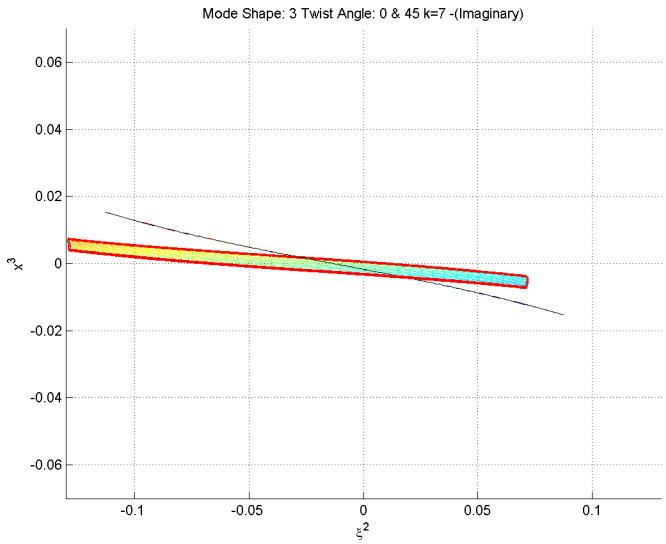

Figure 41: Mode 3 - 45^o Twist Overlay Side View -Imaginary

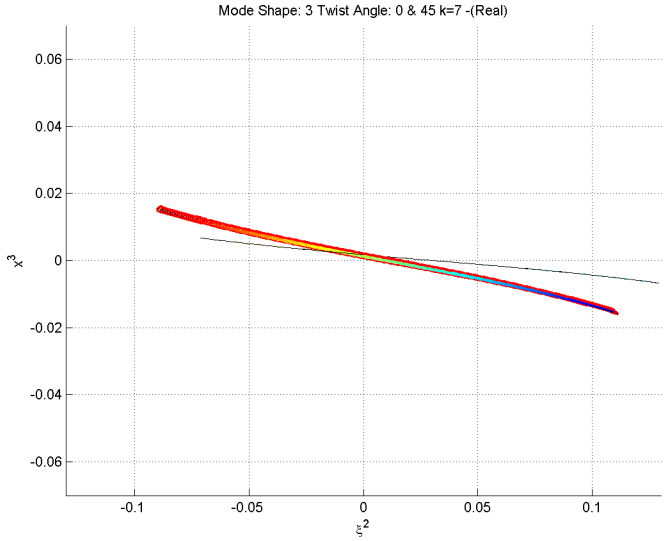

Figure 42: Mode 3 - 45^o Twist Overlay Side View -Real

6.3.4 Bending Modes with respect to Major Axis (ξ^2)

The mode shapes of the bending modes with respect to the major axis show similar deformation to the bending modes with respect to the minor axis, except for the switching of axes. Figures 43-46 illustrate the translation of the cross-section in the ξ^1, ξ^2 -plane.

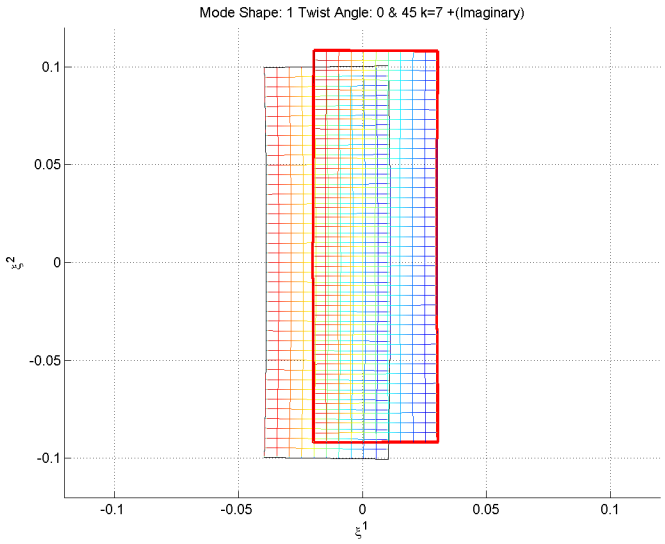

Figure 43: Mode 1 - 45^o Twist Overlay Top View (+Imaginary)

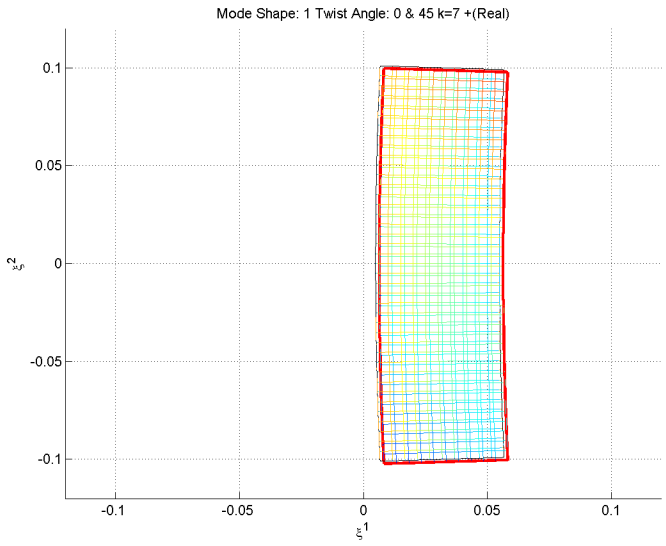

Figure 44: Mode 1 - 45^o Twist Overlay Top View (+Real)

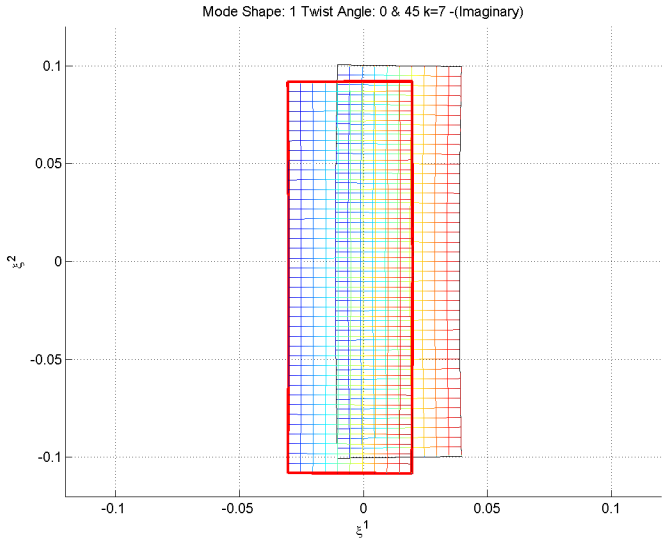

Figure 45: Mode 1 - 45^o Twist Overlay Top View (-Imaginary)

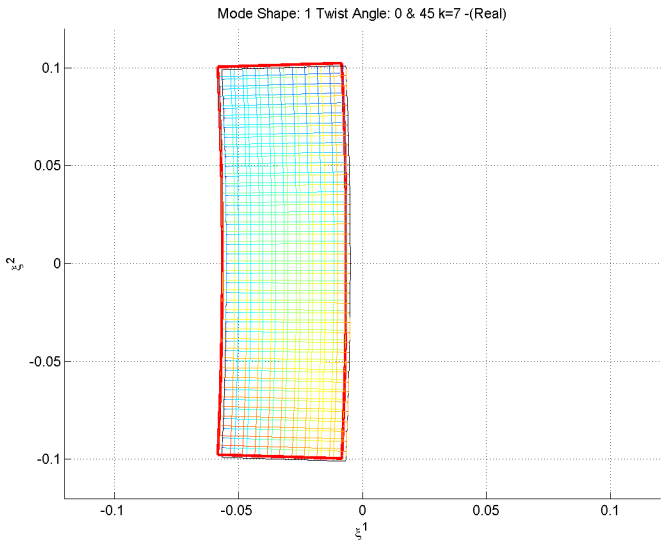

Figure 46: Mode 1 - 45^o Twist Overlay Front View (-Real)

The projections of the mode shapes onto the ξ^1, x^3 -plane are illustrated in Figures 47-50. The typical bending cross-section is observed in the figures. In case of pre-twisted beams, the small rocking with respect to minor axis is superposed.

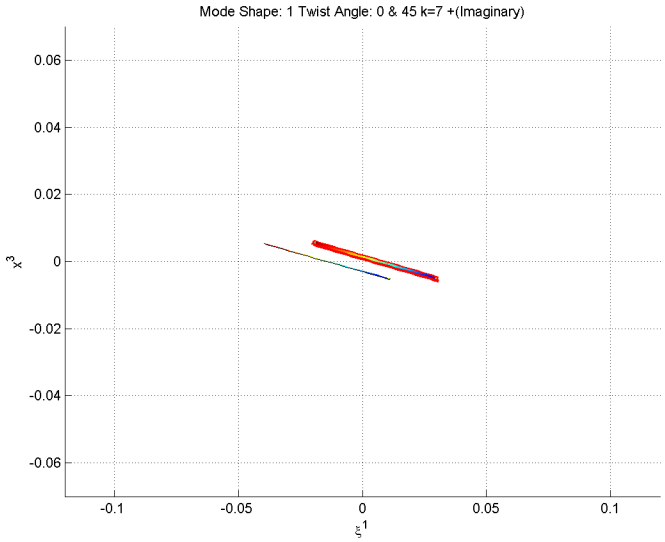

Figure 47: Mode 1 - 45^o Twist Overlay Front View (+Imaginary)

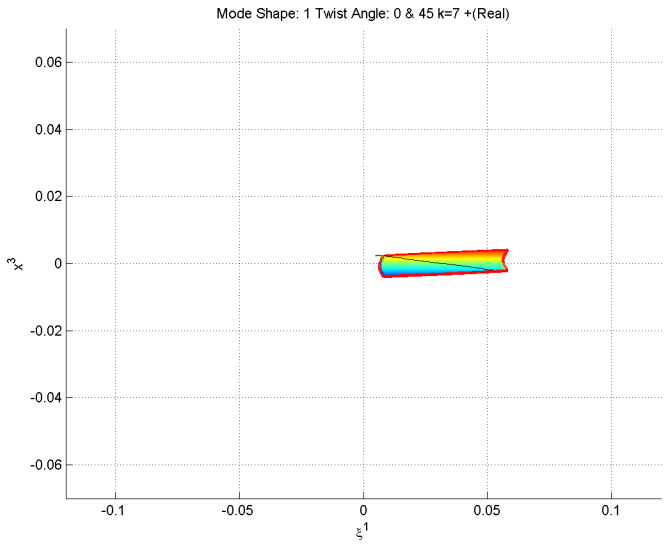

Figure 48: Mode 1 - 45^o Twist Overlay Front View (+Real)

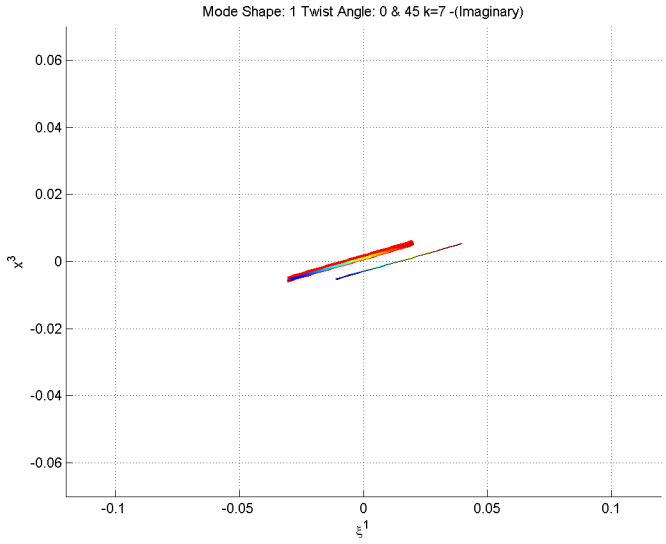

Figure 49: Mode 1 - 45^o Twist Overlay Front View (-Imaginary)

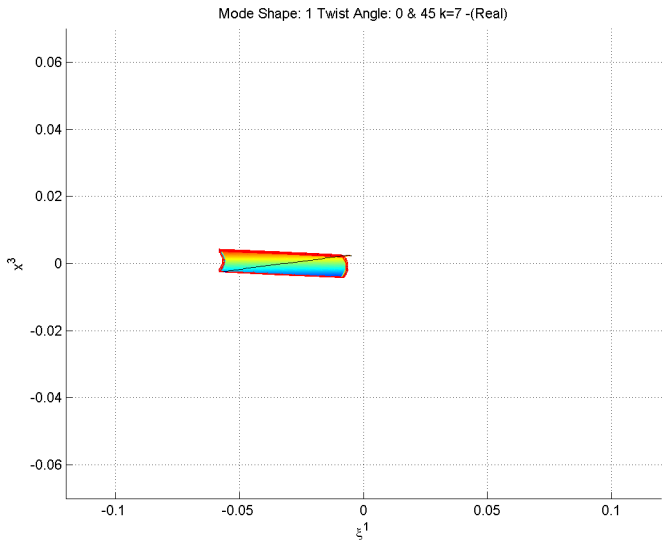

Figure 50: Mode 1 - 45^o Twist Overlay Front View (-Real)

See additional mode shapes in Appendix section

7 Conclusion

A semi-analytical approach to solving wave propagation problem using finite element method has been derived to investigate the dynamic response of pre-twisted beams by obtaining their dispersion relations (k versus ω) and phase velocity spectra (C_p versus k). A study using said method was conducted for three doubly symmetric cross-sections. The lowest four modes which consists of: major bending mode, minor bending mode, torsional mode and longitudinal mode have been identified. Corresponding dispersion relations and phase velocitiy spectra have been obtained and examined. Results shows that the change in pre-twist rate affects the phase velocities of all 4 modes with bending modes being most prominent. Specifically, increasing pre-twist rate lowers the phase velocities of the major bending modes, and elevates the phase velocities of the minor bending modes. The pre-twist effect on torsional and longitudinal modes are much less significant, however, they do seem to become more obvious as aspect ratio increases.

Corresponding mode shapes have also been examined. Findings illustrate that the coupling between minor-major bending modes exist in the pre-twisted beams and is absent in their straight counter parts. Same observation is made for coupling between torsional mode and longitudinal modes.

8 Appendix

8.1 Existing (Pre-twisted) Beam Equations

Equations of motion which aided the interpretation of the phase velocity spectra obtained from finite element method are presented in the following sections:

8.1.1 Banerjee's Pre-twisted Timoshenko Beam:

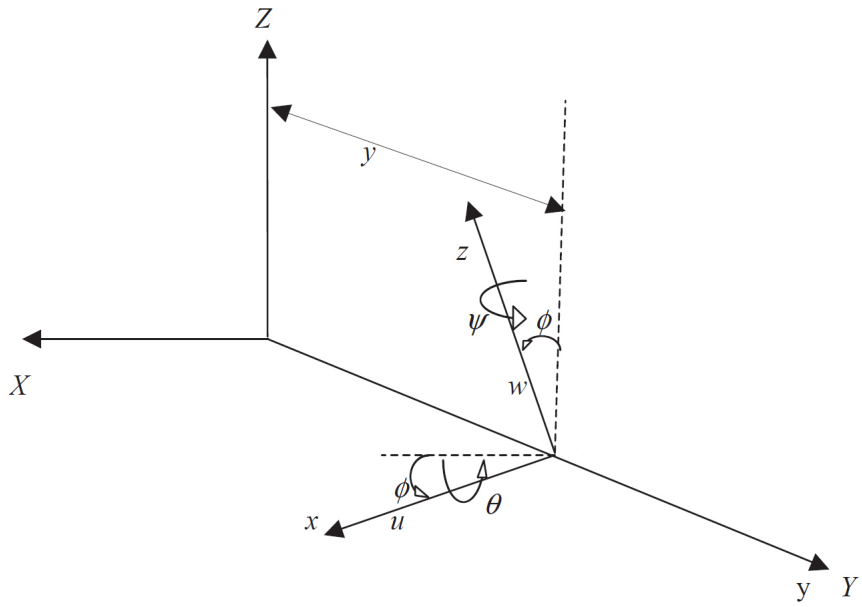

Figure 51: Banerjee's Pre-twisted Beam Notation

Governing equation of motion:

$$
\begin{aligned}
-\rho A\ddot{u} + k_x AGu^{''} - \alpha^2 k_z AGu + \alpha AG(k_x + k_z)w^{'} + k_x AG\psi^{'} - \alpha k_z AG\theta = 0 \\
-\rho A\ddot{w} + k_z AGw^{''} - \alpha^2 k_x AGw - \alpha AG(k_x + k_z)u^{'} - \alpha k_x AG\psi - k_z AG\theta^{'} = 0 \\
-\rho I_x\ddot{\theta} + EI_x\theta^{''} - \alpha^2 EI_z\theta - k_z AG\theta - \alpha k_z AGu + k_z AGw^{'} + \alpha(EI_x + EI_z)\psi^{'} = 0 \\
-\rho I_z\ddot{\psi} + EI_z\psi^{''} - \alpha^2 EI_x\psi - k_x AG\psi - \alpha k_x AGw - k_x AGu^{'} - \alpha(EI_x + EI_z)\theta^{'} = 0
\end{aligned}
\tag{61}
$$

Where u and w are displacements in the local x and z direction. θ and ϕ are the rotation of cross-section with respect to x and z axis. "¨" represents second time derivative. "′" and "″" are derivatives with respect to y/Y direction. α is the angle of twist per unit length in y, ϕ is the angle of twist at y.

If harmonic variation of u, w, θ, and ψ with angular frequency ω and wave number k is assumed then:

$$
\begin{aligned}
u(y,t) &= U_A e^{(iky - i\omega t)} \\
w(y,t) &= W_A e^{(iky - i\omega t)} \\
\theta(y,t) &= \Theta_A e^{(iky - i\omega t)} \\
\psi(y,t) &= \Psi_A e^{(iky - i\omega t)}
\end{aligned}
\tag{62}
$$

Where U_A, W_A, Θ_A and Ψ_A are complex values.

Substituting (62) into (61) and obtain the following system of equations:

$$[K] =$$

$$\begin{bmatrix} -k_x AG(k^2) - \alpha^2 k_z AG & \alpha AG(k_x + k_z)ik & -\alpha k_z AG & k_x AGik \\ -\alpha AG(k_x + k_z)ik & k_z AG(-k^2) - \alpha^2 k_x AG & -k_z AGik & -\alpha k_x AG \\ -\alpha k_z AG & k_z AGik & EI_x(-k^2) - \alpha^2 EI_z - k_z AG & \alpha(EI_x + EI_z)ik \\ -k_x AGik & -\alpha k_x AG & -\alpha(EI_x + EI_z)ik & EI_z(-k^2) - \alpha^2 EI_x - k_x AG \end{bmatrix}$$

$$\left\{ d \right\} = \begin{Bmatrix} U_A \\ W_A \\ \Theta_A \\ \Psi_A \end{Bmatrix}$$

$$[M] = \begin{bmatrix} -\rho A & 0 & 0 & 0 \\ 0 & -\rho A & 0 & 0 \\ 0 & 0 & -\rho I_x & 0 \\ 0 & 0 & 0 & -\rho I_z \end{bmatrix}$$

And:

$$[K] \left\{ d \right\} = \omega^2 [M] \left\{ d \right\} \tag{63}$$

Where k_x and k_z are shear correction factors in the x and z directions. I_x and I_z are area moments of inertia about x and z directions. A is the area of cross-section, E, G, ρ are young's modulus, shear modulus and density of the material respectively.

Resulting eigenpairs from the equations above include 2 bending modes (displacement is dominated by translation) and 2 shearing modes (displacement is dominated by the rotation of the cross-section). In the case of rectangular cross-section with aspect ratio of 4:1, the later 2 modes appear as 6th and 15th mode. These modes are too high to be appropriate for beam assumptions, therefore their phase velocity spectra is ignored from the scope of this thesis.

8.1.2 Other Beam Modes From Elementary Theories:

The phase velocity spectra for 2 other beam modes, namely the longitudinal and torsional modes are obtained using elementary theory. Refer to the notation used in Banerjee's diagram from section above. Adding to it, v is the displacement in y direction (the axis of pre-twist) and ψ is the angle of rotation about the y axis.

Longitudinal:

Equation of motion:

$$\frac{\partial^2 v}{\partial y^2} - \frac{\rho}{E}\frac{\partial^2 v}{\partial t^2} = 0 \tag{64}$$

Using similar derivation as that of the previous section.

$$k = \sqrt{\frac{\rho}{E}}\omega \tag{65}$$

Torsional:

Equation of motion:

$$\frac{\partial^2 \psi}{\partial y^2} JG - I_y \frac{\partial^2 \psi}{\partial t^2} = 0 \tag{66}$$

Where $J = c_2(height)(width)^3$ and $c_2 = 0.281$ for rectangular cross-section of aspect ratio 1:4 (Beer and Johnston [17])

$$k = \sqrt{\frac{I_y}{JG}}\omega \tag{67}$$

8.1.3 Comparison to Existing Beam Theories:

By comparing phase velocity spectra obtained from finite element analysis against those from existing beam theories, the lowest 4 modes are identified and corresponding comparison plots are presented in the following section. These results are obtained at pre-twist rate of $45^o/m$, with beam height h defined as the longer of the two edges in rectangular cross-sections, and twice the major radius in elliptic cross-section.

Banerjee's Timoshenko theory based equations of motion predicted phase velocity reasonably well with an increasing deviation as wave number increases.

Rectangular Cross-Section with Aspect Ratio 4:1

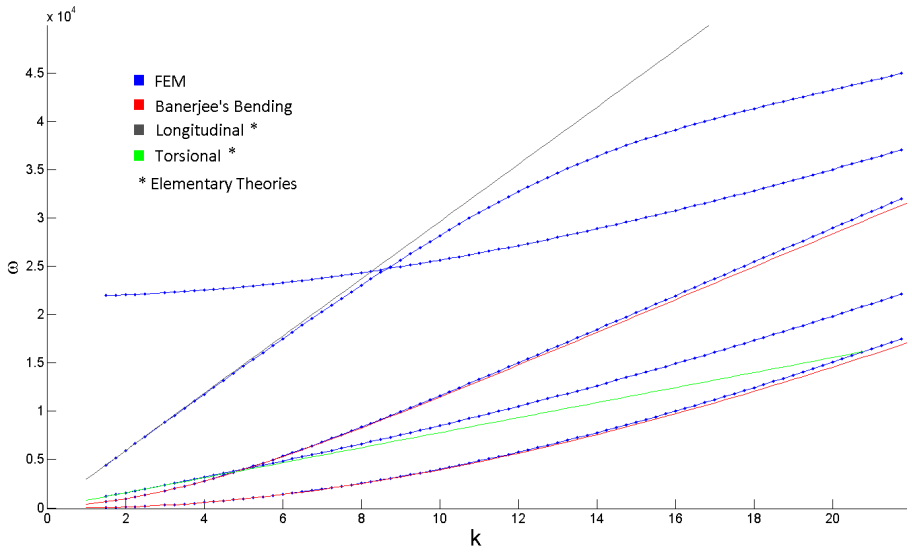

Figure 52: Comparison to Existing Beam Equations - Lowest 4 Modes at $45^o/m$ pre-twist rate (Rectangular 4:1) (ω vs k)

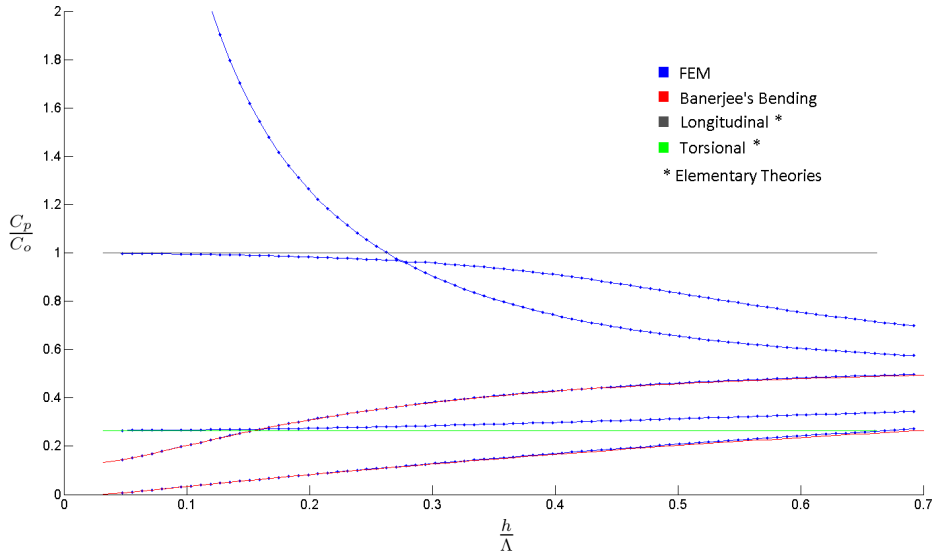

Figure 53: Comparison to Existing Beam Equations - Lowest 4 Modes at $45^o/m$ pre-twist rate (Rectangular 4:1) ($\frac{C_p}{C_o}$ vs $\frac{h}{\Lambda}$)

Rectangular Cross-Section with Aspect Ratio 2:1

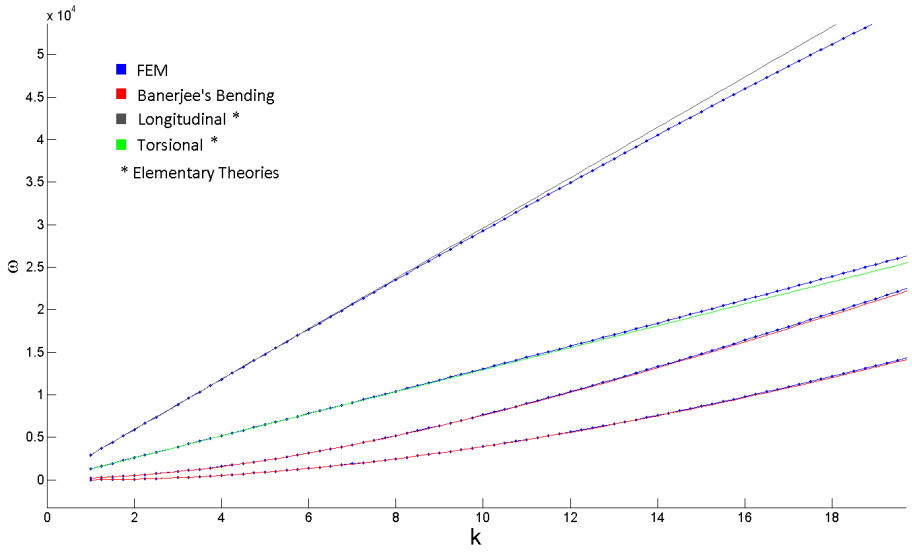

Figure 54: Comparison to Existing Beam Equations - Lowest 4 Modes at $45^o/m$ pre-twist rate (Rectangular 2:1) (ω vs k)

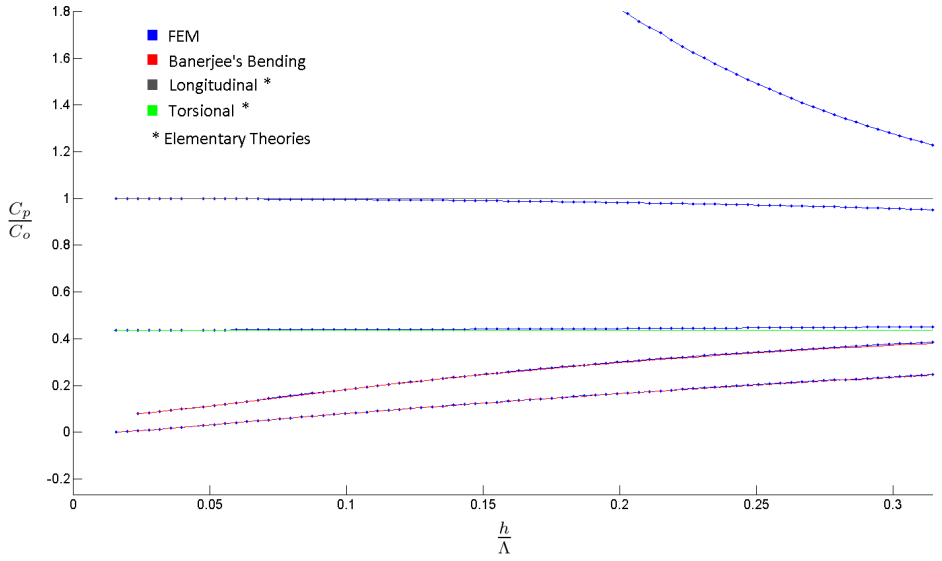

Figure 55: Comparison to Existing Beam Equations - Lowest 4 Modes at $45^o/m$ pre-twist rate (Rectangular 2:1) ($\frac{C_p}{C_o}$ vs $\frac{h}{\Lambda}$)

Elliptic Cross-Section with Aspect Ratio 5:1

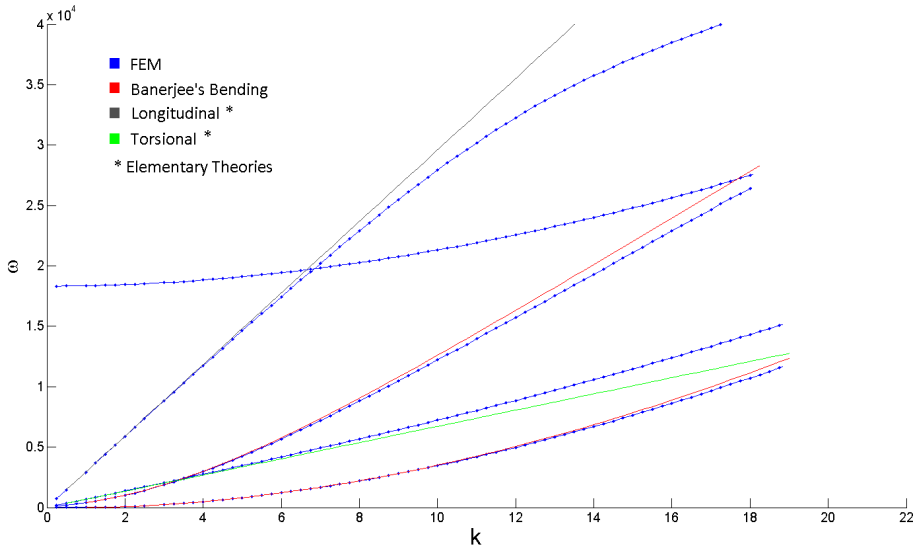

Figure 56: Comparison to Existing Beam Equations - Lowest 4 Modes at $45^o/m$ pre-twist rate (Elliptic 5:1) (ω vs k)

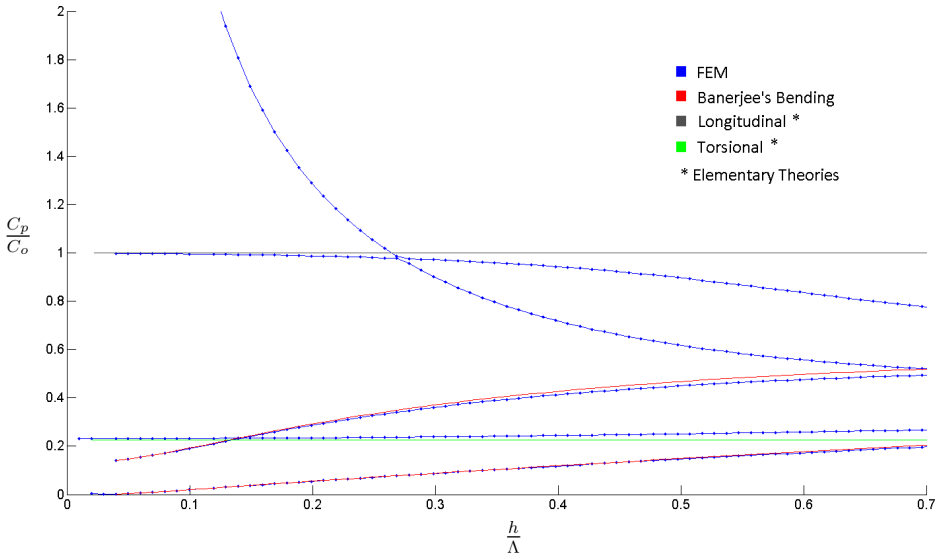

Figure 57: Comparison to Existing Beam Equations - Lowest 4 Modes at $45^o/m$ pre-twist rate (Elliptic 5:1) ($\frac{C_p}{C_o}$ vs $\frac{h}{\Lambda}$)

8.2 Additional Modes

8.2.1 Mode 5:

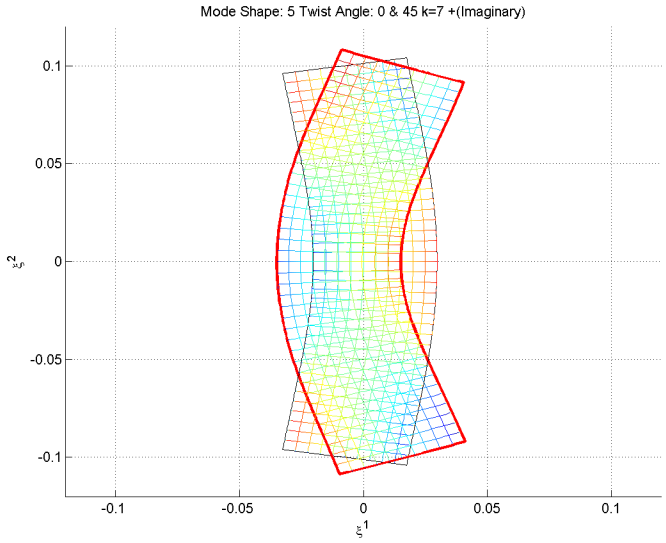

Figure 58: Mode 5 - 45^o Twist Overlay Top View (+Imaginary)

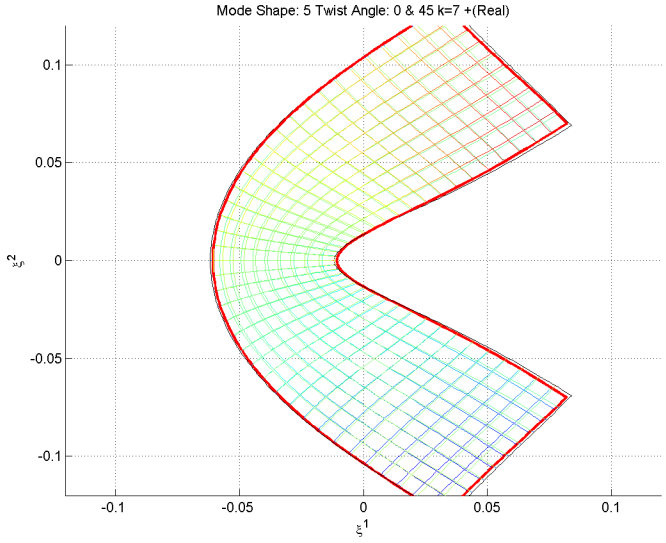

Figure 59: Mode 5 - 45^o Twist Overlay Top View (+Real)

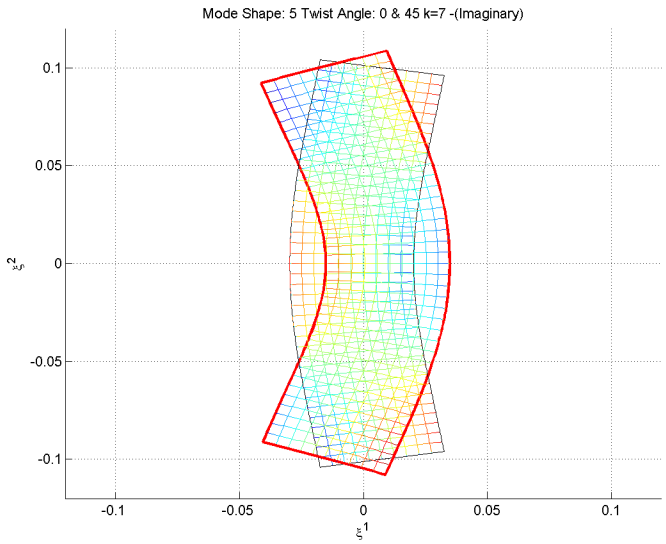

Figure 60: Mode 5 - 45^o Twist Overlay Top View -Imaginary

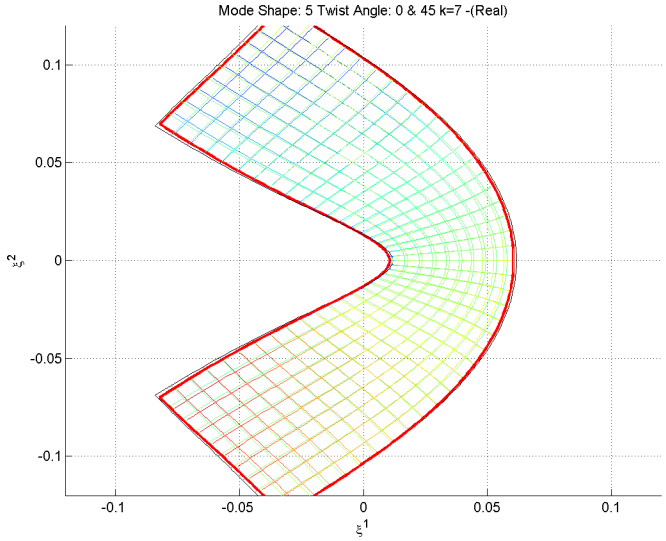

Figure 61: Mode 5 - 45^o Twist Overlay Top View -Real

8.2.2 Mode 6:

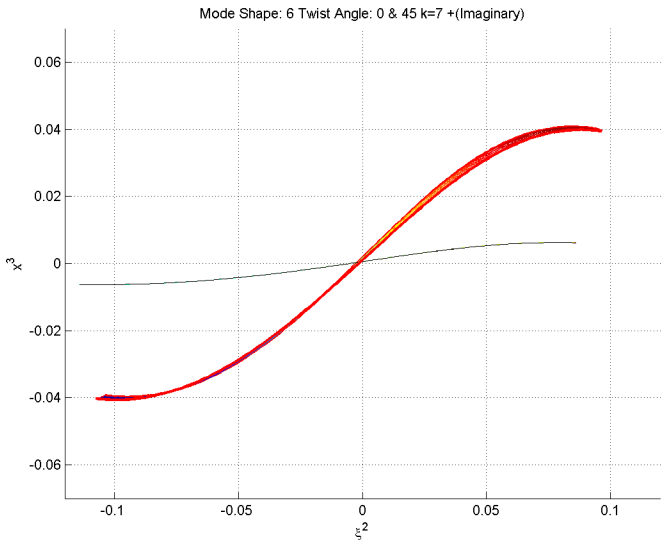

Figure 62: Mode 6 - 45^o Twist Overlay Top View (+Imaginary)

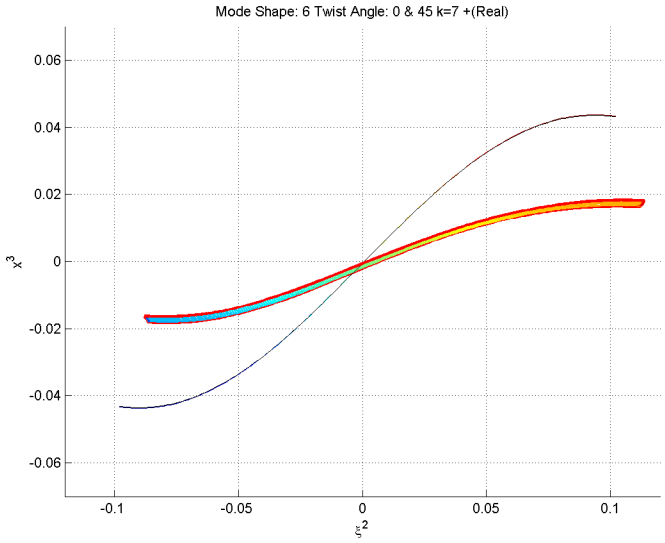

Figure 63: Mode 6 - 45^o Twist Overlay Top View (+Real)

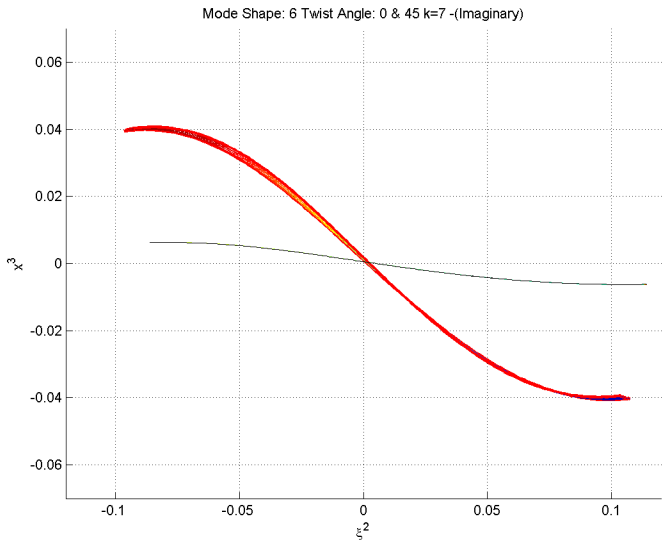

Figure 64: Mode 6 - 45^o Twist Overlay Top View -Imaginary

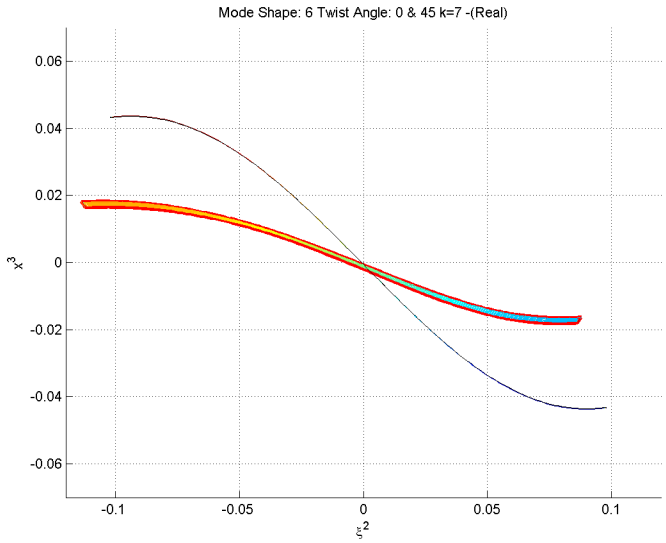

Figure 65: Mode 6 - 45^o Twist Overlay Top View -Real

References

[1] Y.C. Fung and Pin Tong, *Classical and Computational Solid Mechanics*, 2001, World Scientific Publishing, Co. Ltd

[2] J. Yamakawa and H. Murakami, *Longitudinal and Flexural Wave Propagation in Reinforced Concrete Columns*, 1997, International Journal of Solids Structures Vol. 34 Nos 33-34, pp. 4357-4376

[3] H. Murakami and J. Yamakawa, *Torsional Wave Propagation in Reinforced Concrete columns*, 1998, International Journal of Solids Structures Vol. 35 Nos 20, pp. 2617-2637

[4] J.B. Kosmatka, *On the Behavior of Pre-twisted Beams with Irregular Cross-Sections*, 1992, Journal of Applied Mechanics, Vol 59, pp. 146-152

[5] J.N. Goodier and D.S.Griffin, *Elastic Bending of Pretwisted Bars*, 1969, International Journal of Solids and Structures, Vol. 5, pp. 1231-1245.

[6] J.R. Banerjee,*Development of an Exact Dynamic Stiffness Matrix for Free Vibration Analysis of a Twisted Timoshenko Beam*, 2004, Journal of Sound and Vibration, 270(2004)379-401

[7] J.R. Banerjee, *Free Vibration Analysis of a twisted Beam using the Dynamic Stiffness Method*, 2001, International Journal of Solids and Structures, Vol 38, Issue 38-39, pp.6703-6722

[8] T. J.R. Hughes, *The Finite Element Method - Linear Static and Dynamic finite Element Analysis*, 1987, Dover Publication Inc

[9] H.Okubo, *The Torsion and Stretching of Spiral Rods*, 1950, Quarterly of Applied Mathematics, Vol. 9, 263-272

[10] J.C. Buckley, *Bifilar Property of Twisted Strips*, 1914, Philosophical Magazine, Vol. 28, pp. 778-787.

[11] D.H. Hodge, *Torsion of Pretwisted Beams due to Axial Loading*, 1980, Journal of Applied Mechanics, Vol. 47, pp. 393-397.

[12] L. Maunder and E. Reissner, *Pure Bending of Pretwisted Rectangular Plates*, 1957, Journal of the Mechanics and Physics of Solids, Vol. 5, pp. 261-266.

[13] H. Wagner, *Torsion and Buckling of Open Sections*, 1936, NACA TM 807.

[14] K. Washizu,*Some Consideration on a Naturally Curved and Twisted Slender Beam*, 1964, Journal of Mathematics and Physics, Vol. 43, No. 2, pp. 111-116.

[15] A.E. Green and W. Zerna,*Theoretical Elasticity*, 1954, Oxford at the Clarendon Press.

[16] K. Bathe,*Finite Element Procedures in Engineering Analysis*, 1982, Prentice-Hall, inc.

[17] F.P. Beer and E.R. Johnston, *Mechanics of Materials*, 2006, McGraw-Hill.